A combinatorial domain screening platform reveals epigenetic effector interactions for transcriptional perturbation

Hyungseok C. Moon[1]*, Michael H. Herschl[1,2]*, April Pawluk[1], Silvana Konermann[1,3,†], Patrick D. Hsu[1,4,5,†]

[1]Arc Institute, Palo Alto, CA, USA
[2]University of California, Berkeley—University of California, San Francisco Graduate Program in Bioengineering, Berkeley, CA, USA
[3]Department of Biochemistry, Stanford University, Stanford, CA, USA
[4]Department of Bioengineering, University of California, Berkeley, Berkeley, CA, USA
[5]Center for Computational Biology, University of California, Berkeley, Berkeley, CA, USA

*These authors contributed equally: Hyungseok C. Moon, Michael H. Herschl
[†]Correspondence should be addressed to Patrick D. Hsu: patrick@arcinstitute.org or Silvana Konermann: silvana@arcinstitute.org

Abstract

Epigenetic regulation involves the coordinated interplay of diverse proteins. To systematically explore these combinations, we present COMBINE (combinatorial interaction exploration), a high-throughput platform that tests over 50,000 pairs of epigenetic effector domains up to 2,094 amino acids in length for their ability to modulate endogenous human gene transcription. COMBINE revealed diverse synergistic and antagonistic interactions between epigenetic protein domains, including a potent KRAB-L3MBTL3 fusion that enhanced gene silencing up to 34-fold in dose-limited conditions and enabled robust bidirectional CRISPR perturbation. Inducible screening showed DNA methylation modifiers are essential for epigenetic memory, with distinct combinations driving long-term silencing, repression, or activation. Notably, we identified TET1-based combinations that induce hit-and-run upregulation for over 50 days, demonstrating long-term transcriptional activation. This systematic analysis of pairwise domain interactions provides a rich resource for understanding epigenetic crosstalk and developing next-generation epigenome editing tools. More broadly, COMBINE offers a generalizable platform to functionally characterize combinatorial biological processes at scale.

* * *

Introduction

Epigenetic regulation in mammalian cells is a highly coordinated process, essential for organizing genetic information and orchestrating pivotal cellular functions[1] like gene regulation, differentiation, and DNA replication[2] or repair[3]. Central to this regulation are large, multi-protein complexes that control epigenetic states through intricate combinations of post-translational modifications of DNA-scaffolding histone proteins and epigenetic modifications of the genome itself[4]. These complexes often contain numerous subunits with distinct functionalities[5,6], such as the Polycomb repressive complexes[7], that coordinate a complex code of different histone modifications to enable context-dependent control of gene expression and chromatin state.

Inspired by these natural mechanisms, the epigenome editing toolbox leverages similar combinatorial concepts that bring together programmable DNA-binding domains with epigenetic effector proteins[8,9]. For maximal activity, transcriptional activators such as the synergistic activation mediator (SAM) complex fuse a viral activation domain to dCas9 in addition to aptamer-based recruitment of two other activators[10]. Epigenetic silencers such as CRISPRoff or EvoETR have also benefited from combining DNA methyltransferase domains with Krüppel associated box (KRAB) repressors, enabling long-term gene silencing with hit-and-run delivery of the editor system[11–13].

To date, the development of epigenetic editors has largely relied on rational design or low-throughput, guess-and-test approaches[10–23]. Recent advances in pooled gene synthesis have enabled the functional screening of short peptide libraries of ~80 amino acids tiling larger effector protein candidates[24–26], further allowing the annotation of novel bivalent interactions that are synergistic or antagonistic[27]. However, the synthesis length restriction of current-generation oligonucleotide pools may not accommodate the size of functionally active elements, and the use of engineered reporter loci may not extrapolate to endogenous genetic contexts. One recent study used barcoded multicistronic adaptors to clone and screen pairs of transcription factors up to 5.8 kilobases in length using a T cell knock-in system, but the generalizability and scale of this approach is limited by the requirement of a cell-type specific functionally monoallelic target locus and a sharp length-dependent integration bias[28].

To address these challenges, we sought to develop a generalizable high-throughput screening platform to functionally characterize combinations of long and heterogenous epigenetic effectors, with the goal of 1) identifying new effector combinations that increase the potency or durability of transcriptional perturbations, and 2) uncovering previously unknown interactions between individual effector domains.

Here, we report COMBINE (combinatorial interaction exploration), a high-throughput and inducible screening platform that can accommodate heterogeneously-sized fusion elements, including large catalytic domains up to 6.3 kilobases in length. We applied COMBINE to measure the transcriptional perturbation landscape of an endogenous human gene with over 50,000 bivalent epigenetic effectors, composed of pairs of protein domains from diverse classes including readers, recruiters, structural factors, and catalytic writers or erasers.

More than 6,500 bivalent epigenetic effectors were identified as significant hits that perturb the transcription of an endogenous target gene in human cells. Systematic analysis and validation of combinatorial interactions enabled the discovery of previously unknown synergistic or antagonistic interdomain interactions that control epigenetic regulation of transcription in human cells. Our screening data allowed us to nominate new epigenetic effector domain combinations for synthetic biology and genetic medicine, including a potent KRAB-L3MBTL3 fusion that enhanced gene silencing up to 34-fold in dose-limited conditions and enabled a robust bidirectional CRISPR perturbation system to simultaneously activate one target gene and silence another. Examining durable long-term perturbations in our screen, we further identified novel combinations containing CpG DNA methylation-related domains that drive heritable silencing, repression, or activation of an endogenous target gene. COMBINE should be generalizable to a wide variety of lentivirus-transducible cell types and protein domain classes, as well as DNA and RNA elements, providing a broad platform to interrogate biological interactions at scale.

Results

Combinatorial interaction exploration (COMBINE) enables high-throughput bivalent domain screening

Considering the combinatorial nature of epigenetic regulation (**Fig. 1a**), we sought to assess the functional effects of epigenetic domain pairs on gene expression to uncover new biology and potential domain combinations for epigenome editing tools. The limitations of currently available bivalent domain screening technologies necessitated the development of a new pairwise domain screening approach that could accommodate larger domain sizes (many over 1,000 amino acids in length) to assess combinations of epigenetic reader, recruiter, writer, and eraser domains for their effects on gene expression in a high-throughput pooled screen.

To achieve this, we first curated two complementary libraries of epigenetic effectors, each with distinct design principles. Library 1 was designed to identify combinatorial epigenetic repressors and is composed of readers, recruiters, structural factors, writers, and erasers from known repressive epigenetic multiprotein complexes (**Fig. 1b** and **Supplementary Table 1**). It contains a total of 155 domains ranging from 80 aa to 545 aa (**Supplementary Fig. 1a**,**b**). Library 2 was designed to investigate how diverse types of direct epigenetic modifications interact to modulate transcription in both directions (repression or activation). This library is exclusively composed of catalytic writers and erasers of histone and DNA modifications, irrespective of their known effects on transcription (**Fig. 1c** and **Supplementary Table 2**). It contains 198 domains, with a wider size distribution from 100 aa to 1,036 aa (**Supplementary Fig. 1c**,**d**). To mitigate length bias in lentivirus generation, transduction[29], and NGS readout[30], we pooled library members of each library in a weighted fashion and utilized sequential golden gate assembly with CcdB dropout selection to increase cloning efficiency (Methods, **Supplementary Figs. 2** and **3**).

To recruit these epigenetic effectors to an endogenous gene promoter, we used dCas9 targeting in combination with the MS2-MCP aptamer system derived from RNA bacteriophage

144 MS2[31], analogous to our prior designs that utilize sgRNAs with embedded MS2 stem-loops[10,32].
145 For temporal control over the editing complex, doxycycline-inducible promoters drove the
146 expression of both dCas9 and the effector combination fused to monomeric MS2-coat protein
147 (MCP) or synonymous mutated tandem MCP (stdMCP)[33] (**Supplementary Fig. 4a**,**e**). To
148 assess transcriptional outcomes on an endogenous target locus, we chose the gene encoding
149 membrane protein CD81, whose expression can be measured using flow cytometry. We
150 designed a three sgRNA expression cassette targeting upstream of the CD81 transcription start
151 site (TSS) and confirmed the ability to transiently activate and repress CD81 expression with
152 this experimental setup. Using well-characterized effectors including KRAB and the
153 transcriptional activation domain of HSF1, CD81 expression levels showed a good dynamic
154 range of both repression and activation during doxycycline treatment, and returned to baseline
155 at 9 days after the removal of doxycycline (Methods, **Supplementary Fig. 4b-d**,**f-h**).
156
157 For our screen, we transduced the lentiviral libraries encoding Library 1 or Library 2 into K562
158 cells containing Tet-On dCas9 at a low multiplicity of infection (MOI<0.3) with a minimum
159 effector coverage of 100X (Methods, **Fig. 1d** and **Supplementary Figs. 5a** and **6a**). The
160 combinatorial effector was recruited to CD81 loci for 5-6 days by adding doxycycline, followed
161 by cell sorting based on CD81 expression (Day 0 timepoint to evaluate immediate effects on
162 gene expression) (Methods, **Supplementary Figs. 5b-d** and **6b-d**). This was followed by a 12-
163 day effector washout period without doxycycline and a final round of cell sorting (Day 12
164 timepoint to evaluate durable effects on gene expression in the absence of effectors).
165
166 The size differences between Library 1 and Library 2 effector domain combinations (**Fig. 1e**)
167 necessitated different NGS readout strategies. The majority (~82%) of bivalent members in
168 Library 1 fell below the 1500 nucleotide upper limit for short-read NGS platforms[34], enabling us
169 to directly sequence the N- and C-termini of effector pairs using short-read sequencing
170 (**Supplementary Fig. 5a**). In contrast, Library 2 often exceeded this limit. To overcome this, we
171 included a short 20N barcode in the cloning process, which was initially mapped to the effector
172 pair by nanopore sequencing and read out by short-read sequencing at the end of the screen
173 (Methods, **Supplementary Figs. 3g-k** and **6a**,**e**). Targeted nanopore sequencing of integrated
174 Library 2 members indicated less than 10% barcode swapping (**Supplementary Fig. 7**). Our
175 barcoded approach with exponential effector pooling for Library 2 resulted in a reduction of the
176 Day 0 dropout rate from 42.9% in Library 1 to 4.2% and successfully offset the exponential
177 decay of effector coverage with increasing length that was observed for Library 1 and previous
178 combinatorial screening approaches (**Supplementary Fig. 8a,d**)[28,35]. Effector dropout on Day
179 12 remained consistent at 42.1% for Library 1 and increased to 19.3% for Library 2
180 (**Supplementary Fig. 8b**,**c**,**e**).
181
182 The transcriptional effects of each domain combination were determined by measuring the
183 relative abundance of each unique effector pair in the sorted cells from the high and low CD81
184 expression bins, calculated as $\log_2$ fold enrichment. Both libraries effectively captured the
185 temporal dynamics of CD81 transcriptional perturbation induced by well-established control
186 effectors. In Library 1, target gene repression by combinations containing the KRAB domain
187 from ZNF10 was strong at Day 0 and disappeared by Day 12 ($\log_2$ fold score of -4.7 and -0.24,

188 **Fig. 1f**,**g** and **Supplementary Table 3**). Similarly, repression by full-length RYBP, a known
189 epigenetic silencer that recruits Polycomb repressive complex 1 (PRC1)[36], and activation by the
190 activation domain of HSF1 were captured at Day 0 and dissipated by Day 12 after dox removal
191 for Library 2 (average $\log_2$ fold scores of -3.6 and 0.083 for RYBP and 1.9 and 0.047 for HSF1,
192 **Fig. 1h**,**i** and **Supplementary Table 4**). Based on both CD81 expression levels measured by
193 flow cytometry and HTS enrichment scores (**Supplementary Fig. 5c** and **Supplementary**
194 **Tables 3** and **4**), the majority of transcriptional effects disappeared by 12 days after the removal
195 of doxycycline (Day 12), highlighting the transient nature of perturbations introduced by the
196 majority of epigenetic and transcriptional modifiers.
197

198 **COMBINE generates rich combinatorial landscapes of pairwise epigenetic**
199 **interactions**

200 To visualize transient perturbation outcomes across the large space of combinations tested, we
201 generated enrichment score heatmaps (**Fig. 2a**,**b** and **Supplementary Fig. 9**). We observed
202 clear diagonal symmetry between the X-Y and Y-X orientations of the same two effectors, with a
203 high degree of correlation across pairs, indicating that most effector pairs behaved similarly
204 regardless of orientation (Library: 1 r = 0.75; Library 2: r = 0.69, **Supplementary Fig. 10**).
205
206 To identify general trends for the transcriptional impact of effector classes, we grouped pairs
207 based on the families of individual effectors (**Fig. 2c,d**). While Library 1 revealed the strongest
208 repressive phenotypes among KRAB family pairs, Library 2 revealed strong repression across
209 pairs of histone deacetylases (HDACs) and DNA methyltransferases (DNMTs). We also
210 observed a surprising trend toward mild target gene repression with pairs of DNA demethylation
211 machinery (DNDM) domains. Pairs of histone acetyltransferases (HATs) tended to activate
212 gene expression, as did histone deubiquitinases (DUBs) despite their ability to remove both
213 activating and repressive histone ubiquitination marks. Finally, pairs of histone lysine
214 methyltransferases (HKMTs) and histone kinases (HKs) ranged broadly across both activation
215 and repression outcomes.
216
217 Next, we examined the directionality of individual effectors in the context of these class-level
218 trends. In the HAT class, pairs containing C-terminal EP300 (a broad HAT capable of
219 acetylating all four core histones[37]) tended to activate transcription, whereas combinations
220 containing C-terminal CDY1 (which displays a strong acetylation preference for histone H4[38])
221 tended to repress transcription (**Fig. 2e**). In addition, some HAT effectors, such as KAT6A or
222 KAT14 (a broad histone and weak H4 acetyltransferase, respectively[39,40]), exhibited more
223 partner-dependent effects.
224
225 Compared to the HAT class, the HDAC domain class had more members that consistently
226 repressed transcription irrespective of their N-terminal partners such as SIRT1 (a broad histone
227 deacetylase and decrotonylase[41]) and class IIa HDACs (HDAC5, HDAC4, and HDAC7, **Fig. 2f**).
228 However, the degree of repression ranged widely depending on the exact effector pairing. For
229 example, the combination of EP300 and HDAC5 activated transcription with an average $\log_2$
230 fold enrichment of 1.1, while the pairing of UBE2E1 and HDAC5 repressed transcription with a

231 score of -4.5. These global observations motivated us to quantitatively analyze the contribution
232 of individual domain effects and domain-domain interactions to gene expression outcomes.
233
234 **Marginal effector analysis reveals how individual domains affect transcription**
235 **irrespective of partners**
236 To quantitatively assess how each of the individual effector domains in our two libraries
237 contribute to epigenetic control of gene expression, we calculated a 'marginal effector score' for
238 each domain (**Fig. 3a**,**b**). This score reflects the average enrichment value across all bivalent
239 combinations containing the domain of interest relative to all combinations lacking it, yielding a
240 measurement of each domain's relative contribution to target gene expression (positive or
241 negative) across pairings.
242
243 Marginal effector analysis of Library 1 clearly reflected the well-known repressive effect of KRAB
244 domains on gene expression[16,24]. The average marginal score across the KRAB domain class
245 was -3.8, indicating an average 14-fold decrease in enrichment scores when KRAB is present in
246 an effector pair ($2^{3.8} \approx 14$, **Fig. 3c** and **Supplementary Table 3**). The ZNF10 (KOX1) KRAB
247 domain – which is commonly used in CRISPR interference (CRISPRi) applications[42] – exhibited
248 the lowest marginal score at -5.8. The more recently identified ZIM3 KRAB domain also
249 exhibited strong repression with a score of -4.5[20]. Notably, only two out of 25 tested KRAB
250 domains did not consistently repress gene expression (ZNF791 and ZNF823; marginal scores
251 of -0.1 and 1.0), suggesting that this family contains a wide spectrum of additional potential tool
252 domains that have yet to be explored.
253
254 Outside the KRAB domain family, we identified two other individual domains with significantly
255 repressive marginal scores in Library 1: SID4X (marginal score -4.3) and the sterile alpha motif
256 (SAM) domain of L3MBTL3 (marginal score -1.1). SID4X is an engineered ternary version of the
257 Sin3 interacting domain (SID) from the MAX dimerization protein 1 (MXD1) that efficiently
258 recruits the Sin3-HDAC complex[43], and the SAM domain of L3MBTL3 is known to multimerize
259 and recruit lysine-specific histone demethylase 1A (LSD1/KDM1A)[44,45], providing clear
260 mechanistic hypotheses for the repressive effects of each of these domains.
261
262 To independently validate each domain's individual contribution to transcriptional repression
263 outside of the bivalent effector context, we fused ZNF10 KRAB, SID4X, or L3MBTL3 SAM to
264 stdMCP and expressed them in the Tet-On dCas9 K562 cell line alongside a CD81-targeting
265 guide array (**Fig. 3d**). Repression of CD81 target gene expression, as measured by the change
266 in total mean fluorescence intensity (MFI), correlated with each domain's relative marginal effect
267 score: ZNF10 KRAB decreased CD81 MFI by 99%, SID4X by 90%, and L3MBTL3 by 46%
268 relative to the negative control. Notably, unlike the all-or-nothing silencing pattern of KRAB[16],
269 neither SID4X nor L3MBTL3 fully silenced CD81, but rather resulted in more graded repression.
270
271 The marginal scores calculated from Library 2 were lower in magnitude, likely reflecting the
272 more varied composition of this library in comparison to the repression-focused Library 1 (**Fig.**
273 **3e** and **Supplementary Table 4**). At the class level, the DNMT class exhibited the highest

average repression, with a moderate effect size but high consistency across members (average marginal score -0.87). The DUB class resulted in the highest average gene activation with moderate but consistent effects (average marginal score 0.47). At the individual effector level, five of the seven top repressive domains in Library 2 belonged to the HDAC class (including HDAC7 and HDAC4 with scores of -2.2 and -2.1, respectively), while the HAT class contained the two strongest individual activators (EP300 and KAT5 with scores of 1.8 and 1.6, respectively).

Next, we confirmed the effects of 5 individual domains by fusing them to MCP and transiently expressing them in the same cell line used above. The strongest repressor, HDAC7 (marginal score -2.2), reduced CD81 MFI the most, by 64%, and was modulated by the introduction of point mutations (**Fig. 3f**). The hyperactive H843Y mutant[46] increased repression to 82%, and the hypoactive H670L mutant[47] diminished repression to 48% (Methods, **Supplementary Table 5**). Three additional repressors from diverse classes also repressed CD81 in concordance with their marginal scores. RAG1 (marginal score -0.72), an E3 ubiquitin ligase (E3 UBL) associated with histone H3 monoubiquitination during V(D)J recombination[48,49], repressed CD81 by 39%; UBE2E1 (marginal score -0.69), an E2 ubiquitin ligase (E2 UBL) associated with PRC1[50], repressed CD81 by 35%; and KMT5B (marginal score -0.12), a histone lysine methyltransferase (HKMT) that writes H3K20 methylation[51] – a modification for which no targeted epigenetic editing tools currently exist, repressed CD81 by 32% (**Fig. 3g**). Catalytic mutations of these three enzymes[52–54] reduced CD81 repression to 24%, 9%, and 10% respectively.

For activation, KAT5 (marginal score 1.6) was the second-ranking activator of gene expression in the screen, and validation experiments confirmed that it resulted in a 15% increase in CD81 MFI (**Fig. 3g**) which was completely abolished upon introduction of a catalytic point mutation. Altogether, our marginal effector analysis and validations of domains from Library 2 indicated a wide range of repressive and activating effects.

COMBINE reveals synergy and antagonism in epigenetic domain interactions

Beyond the effects of individual domains on target gene expression, a key advantage of COMBINE is the ability to quantify synergistic or antagonistic interactions among domain pairs. To systematically assess domain interactions, we calculated a ‘synergy score’ for each effector pair that uses individual marginal scores to calculate the difference between expected and observed effector strength for each domain combination (Methods, **Fig. 4a**). Positive scores indicate synergy and negative scores indicate antagonism in the direction of the stronger marginal effector. Across both libraries, we identified many strong synergistic or antagonistic interactions between domains that provide a rich resource for further exploration (**Supplementary Figs. 11** and **12** and **Supplementary Tables 6** and **7**). Compellingly, our analysis highlighted synergistic interactions between several PRC1 recruiters and a reader of H2AK119 monoubiquitination, recapitulating the known reader-writer synergy of variant PRC1 (**Supplementary Fig. 13** and **Supplementary Note 1**)[36].

We were intrigued by the broad interaction patterns observed across the robust repressive domain classes, KRAB and HDAC. When analyzing the synergy scores for all KRAB and HDAC

318 members with clear individual repressive effects (marginal scores below -0.5, **Supplementary**
319 **Fig. 14**), we were able to classify additive, synergistic, and antagonistic effector pairings with
320 other library members. For example, we observed that the strongly activating HAT members
321 KAT5 and EP300 fully canceled out the repressive effect of HDACs in a way that was explained
322 by a direct additive relationship (**Fig. 4b**). In contrast, 46 effectors resulted in synergistic
323 enhancement of repression by HDAC domains (**Supplementary Table 7**). We selected two
324 pairs with particularly high synergy scores for experimental validation: HDAC7 + UBE2E1
325 (synergy score 2.4) and HDAC4 + VRK1 (synergy score 2.0).
326
327 In validation experiments, we found that the HDAC7 + UBE2E1 and HDAC4 + VRK1
328 combinations reduced CD81 MFI by 75% and 73%, respectively, relative to the neutral control.
329 This enhanced repressive effect was at least partially dependent on the catalytic activities of
330 both effectors, as hypoactive mutations in the HDAC partners[47] reduced each combination's
331 repression level to 63% and 36%, respectively, while loss-of-function mutations in the UBE2E1
332 and VRK1 partners[53,55] attenuated repression to 57% and 48%, respectively (**Fig. 4c**,**d**).
333 Installing hyperactive mutations into the HDAC partner[46] boosted CD81 repression to 92% for
334 both combinations, further emphasizing the role of HDAC catalytic activity in this outcome.
335
336 As an E2 UBL associated with PRC1, UBE2E1 participates in the ubiquitination of H2AK119 to
337 promote gene repression[50]. We hypothesize that gene repression by HDACs is enhanced by
338 these epigenetic effectors since the removal of histone acetylation marks near the CD81 locus
339 (**Supplementary Fig. 15a**)[56] could increase the efficiency of writing repressive marks through
340 established PRC crosstalk mechanisms[4]. While future mechanistic studies are needed, these
341 results demonstrate the ability of our combinatorial screening platform to generate novel
342 mechanistic hypotheses about fundamental biological processes.
343
344 To address the generalizability of our potent HDAC combinations as well as individual domains
345 identified from Library 2, we tested 13 key effectors on a panel of 4 additional basally expressed
346 genes including CD55, CD58, CD151, and CD155. Five days post-nucleofection of both effector
347 and 3X guide array plasmids, we observed that the percent changes in MFI for each of the
348 effectors were similar across all tested genes (**Fig. 4e** and **Supplementary Fig. 16**). The
349 percent changes were highly correlated between genes, spanning a range of r = 0.87-0.98 and
350 demonstrating that our findings are broadly applicable to other target genes (**Fig. 4f** and
351 **Supplementary Fig. 17**).
352
353 Next, we examined synergy scores among the KRAB family of repressive domains to discern
354 partner domains that could enhance or antagonize KRAB activity. Our synergy score analyses
355 identified the SAM domain from L3MBTL3 and two PRC2 recruiters (PALI1 and EPOP) as the
356 most potent synergistic partners of KRAB domains, all exhibiting both high average synergy
357 scores and low enrichment scores on Day 6 (average synergy scores 4.0, 2.0, and 1.7 and $\log_2$
358 fold enrichments -5.7, -3.7, and -3.4, respectively) (**Fig. 4g**, **Supplementary Fig. 11b** and
359 **Supplementary Table 6**). In individual validation of these domain combinations, all three KRAB
360 combinations – L3MBTL3, PALI1, and EPOP – further enhanced repression of CD81 compared

361 to the ZNF10 KRAB domain alone (L3MBTL3 + KRAB, KRAB + PALI1, GFP + KRAB were
362 97.7%, 86.6%, and 65.6% of CD81-repressed cells, **Fig. 4h** and **Supplementary Fig. 18a**,**b**).
363
364 PALI1 and EPOP are vertebrate-specific and mutually exclusive PRC2 subunits[57] that can
365 recruit the PRC2.1 complex, thereby promoting the deposition of H3K27 trimethylation[58]. In our
366 screen, the PRC2 interacting domains (PID) of PALI1 [1058 - 1250 aa] and EPOP [300 - 379
367 aa] exhibited synergy with KRAB. KRAB + PALI1 PID and KRAB + EPOP PID combinations are
368 expected to install both H3K9 methylation marks via KRAB and H3K27 trimethylation marks
369 through recruitment of PRC2. Notably, in its endogenous context, the full-length PALI1 protein
370 [1 – 1557 aa] is also capable of installing both H3K9 and H3K27 methylation marks, as it
371 contains both the H3K9 methyltransferase G9A interacting domain [310 - 723 aa] and PRC2
372 interacting domain [1058 - 1250 aa][59]. Considering that both G9A and KRAB zinc-finger proteins
373 are vertebrate-specific proteins, synergistic interactions with vertebrate-specific components of
374 PRC2 complexes raises interesting questions about the co-evolution of epigenetic components.
375 Overall, we demonstrate the ability of COMBINE to highlight naturally occurring synergistic
376 combinations of epigenetic domains.
377

378 KRAB + L3MBTL3 combination enables potent transcriptional repression in 379 challenging conditions

380 Individual KRAB domains, including those of ZNF10 and ZIM3, have been harnessed as
381 epigenetic repressors in many contexts[20,42] and yielded strong individual marginal scores in our
382 screen (-5.8 and -4.5, respectively). However, in certain contexts – for example, under dose-
383 limited conditions due to viral delivery, or when recruited to a locus in a more indirect manner –
384 further enhancement of repressive activity would be beneficial. To provide new tool options for
385 these challenging conditions, we examined our screen data for synergistic combinations that
386 would enhance the potency of these KRAB domains.
387
388 In our screen data as well as in individual validation, the synergistic pairing of ZNF10 KRAB with
389 the SAM domain from L3MBTL3 was the most potent combination identified. Notably, the SAM
390 domain is known for its ability to multimerize[44], potentially recruiting multiple KRAB domains to
391 the target gene (**Fig. 5a**). We tested this combination under dose-limiting conditions using low
392 MOI lentiviral transduction of K562 cells with either the stdMCP-KRAB or stdMCP-KRAB-
393 L3MBTL3 effectors combined with a single sgRNA – instead of three – targeting CD81
394 (**Supplementary Table 8**). We observed significantly enhanced repression of the combined
395 KRAB + L3MBTL3 effector under these challenging conditions, particularly at low levels of
396 doxycycline induction where we achieved up to ~34-fold increased repression (KRAB: 1.4% vs
397 KRAB + L3MBTL3: 48.1% at 5 ng/μL dox) (**Fig. 5b**). Even at standard 1000 ng/μL doxycycline
398 conditions, the KRAB + L3MBTL3 combination exhibited ~6-fold increased repression compared
399 to KRAB alone.
400
401 To test the generalizability of this effect, we selected three additional gene targets encoding cell
402 surface proteins with basal expression in K562 cells (CD55, CD58, and CD151). The KRAB +
403 L3MBTL3 effector consistently demonstrated superior repression across three additional target
404 genes compared to KRAB alone (**Fig. 5c**), ranging from 1.2-fold improvement with the highly

405 effective CD151 targeting sgRNA to 8.0-fold for a weaker CD81 targeting sgRNA. Together,
406 these results support the ability of this domain combination to overcome the limitations of
407 weaker sgRNAs or lower effector expression to achieve robust repression across diverse target
408 genes.
409
410 Beyond the general enhancement of CRISPRi activity in challenging settings, we reasoned that
411 the increased efficacy afforded by the KRAB + L3MBTL3 combination could be particularly
412 enabling for bidirectional CRISPR perturbations, in which two orthogonal epigenetic effectors
413 can be targeted to two distinct loci to achieve upregulation of one gene and simultaneous
414 repression of another[10,60,61]. To assess this possibility, we used the stdMCP fusion strategy to
415 recruit KRAB alone or KRAB + L3MBTL3 to an MS2-containing CD81 sgRNA or non-targeting
416 control guide, while using an analogous setup to recruit the p65-HSF1 CRISPRa effector[62] using
417 the orthogonal stdPCP-PP7 system[33,60]. We engineered cell lines to express dCas9, stdMCP-
418 KRAB or stdMCP-KRAB-L3MBTL3, and stdPCP-p65-HSF1 in a doxycycline-inducible manner
419 and introduced four dual MS2/PP7 sgRNA combinations – each containing either a CD81-
420 targeting or a non-targeting MS2 sgRNA paired with a CD274-targeting or a non-targeting PP7
421 sgRNA – using lentivirus.
422
423 Importantly, we found that the KRAB + L3MBTL3 combination fully silenced CD81 expression to
424 produce four distinct populations, unlike the KRAB-only condition (**Fig. 5d**,**e**). This improved
425 separation resulted from augmented repression by the KRAB + L3MBTL3 combination (KRAB:
426 41.5% vs KRAB + L3MBTL3: 89.4% CD81 repressed cells) without interfering with CD274
427 activation by the PP7 system (KRAB: 66.5% vs KRAB + L3MBTL3: 74.5% CD274 activated
428 cells) (**Supplementary Fig. 19**). The KRAB + L3MBTL3 combination therefore enabled us to
429 overcome limitations in the efficacy of other MS2-based repressors and develop a robust
430 MS2/PP7-based bidirectional perturbation system, which may be applied to future bidirectional
431 CRISPR screening[63,64] or therapeutic applications.
432

433 **Long-term epigenetic memory requires modifiers of DNA methylation**

434 Thus far, we have demonstrated the power of COMBINE to identify new individual effectors and
435 combinations of effectors that transiently perturb gene expression, accurately measuring
436 effector strength and uncovering unexpected synergistic and antagonistic interactions. Next, we
437 investigated durable effects on target gene expression produced by transient expression of the
438 epigenetic editing complex (**Fig. 6a**). Following the initial 5-6 day effector recruitment phase,
439 doxycycline was removed to halt any further production of dCas9 and the (std)MCP-fused
440 effectors. Using our pilot studies as a reference, in which short-term repression by KRAB
441 dissipated after twelve days (**Supplementary Fig. 4b**-**d**), we cultured cells for twelve days
442 following doxycycline removal to our final screening timepoint. By Day 12, the majority of
443 transcriptional effects had dissipated (**Fig. 1g**,**i** and **Supplementary Tables 3** and **4**).
444
445 Implementing the marginal score metric that we developed earlier allowed us to quantitatively
446 determine the magnitude of long-term changes to target gene expression induced by each
447 individual effector across different combinations. Across both libraries, only three individual
448 effectors induced significant long-term transcriptional changes with absolute marginal scores

449 greater than 0.5, and all of these effectors participate in DNA methylation (**Fig. 6b** and
450 **Supplementary Fig. 20a**). Two of the identified effectors, DNMT3A-3L[17] and DNMT3A, stably
451 repressed target gene expression, while one effector, TET1, stably activated target gene
452 expression. In contrast to DNMT3A-3L and DNMT3A, which are capable of *de novo* methylation
453 of CpG sites[65–67], TET1 oxidizes methylated cytosines to promote DNA demethylation[67,68].
454 Notably, both DNMTs have been shown to induce long-term silencing[12,17,19], while TET1 has
455 been used to reactivate disease-relevant or synthetically silenced genes in long-term[12,69] and
456 upregulate target gene expression in a transient manner[67,70,71]. Implementing our synergy score
457 metric on Day 12 screen data recovered the established synergistic interaction between the
458 KRAB domain and DNMT3A – the basis for CRISPRoff technology[11,12] – as the strongest hit in
459 Library 1 (**Supplementary Fig. 20b**,**c**).
460
461 We followed up on each of these three domains - including different pairings suggested by our
462 screen data - with individual validation experiments. DNMT3A-3L exhibited moderate but stable
463 long-term repression both individually as well as in combinations identified to induce repressive
464 memory in the screens (DNMT3A-3L, UHRF1 + DNMT3A-3L, PRDM4 + DNMT3A-3L, 23.4%,
465 19.7%, and 18.5% of cells repressed 12 days after doxycycline removal, respectively, **Fig. 6c**
466 and **Supplementary Fig. 21a**-**d**). This repression was sustained for up to 50 days. We further
467 tested a hypoactive mutant of UHRF1 and an inferred hypoactive mutant of PRDM4, mutating a
468 conserved tyrosine that is catalytically active in closely related PRDM9[72,73]. Incorporating these
469 mutations led to a 1.4-fold and 2.4-fold reduction in repression on average over the 50-day
470 timecourse (**Supplementary Fig. 21e**). The RING finger domain of UHRF1 is an E3 UBL that
471 catalyzes ubiquitination of H3K18 and H3K23, which in turn recruits and stimulates DNMT1 to
472 faithfully maintain DNA methylation[74–77]. It follows that DNMT1 may aid DNMT3A-3L in
473 establishing methylation patterns that are heritable, for example by converting *de novo*
474 hemimethylated CpGs into fully methylated CpGs.
475
476 For DMNT3A, we selected the combination with UBE2E1 for individual validation. Interestingly,
477 we observed that this combination led to minimal complete silencing (2.1% cells fully silenced at
478 12 days), but did result in a 40.5% reduction in mean CD81 expression across all cells
479 (measured as MFI) at 12 days, which lasted up to 50 days (**Fig. 6d** and **Supplementary Fig.**
480 **22a**-**c**). Notably, this effect was reduced by 2.3-fold when UBE2E1 was mutated at its catalytic
481 cysteine and completely abolished when DNMT3A was catalytically inactivated
482 (**Supplementary Fig. 22d**)[53,78]. These results indicate that DNMT3A is the primary mediator of
483 this repressive epigenetic memory, but that UBE2E1 augments DNMT3A's activity, at least
484 partially through its catalytic function as an E2 UBL. The ability to stably reduce gene
485 expression without silencing will enable future functional genomics studies interrogating gene
486 dosage as well as offer therapeutic downregulation of genes in situations where maintaining low
487 levels of target gene expression is required.
488
489 In addition to long-term repression, we observed long-term epigenetic activation catalyzed by
490 TET1 combinations. While TET1 has been previously used to reactivate the expression of target
491 genes silenced by DNA methylation in synthetic or disease contexts[12,69], our marginal effector
492 score analysis suggests that TET1 can also increase the expression of a basally expressed

target gene not only transiently[67,70,71] but also in a long-term manner. For individual validation, we selected the three TET1 partners with the highest activation from our screen - RNF20's RING finger domain, SMYD1's SET domain, and PRDM1's PR/SET domain. All three TET1 combinations led to an increase in CD81 expression that lasted up to 50 days and reached 40.3%, 28.7%, and 35.6% respectively at 6 days post-doxycycline washout (**Fig. 6e** and **Supplementary Fig. 23**). Activation by TET1 alone, on the other hand, only lasted up to 21 days and reached 19.5% at day 6. Mutation of the known catalytic residues of TET1 not only abrogated the activation phenotype[68] but surprisingly led to stable gene repression, while catalytic mutations in the TET1 partners had a neutral or positive effect on long-term activation compared to their unmutated counterparts (**Supplementary Fig. 24**). These results indicate that other as-yet unknown factors, such as for example the recruitment of endogenous machinery, can augment long-term activation induced by TET1.

In summary, we delineated three distinct modes of epigenetic memory mediated by modulators of DNA methylation: silencing, reduction in gene expression, and activation (**Fig. 6f**). We further demonstrate the ability to tune the degree of long-term repression on endogenous genes and establish long-term activation of a basally expressed gene on a single cell level. Future work will delineate the mechanistic differences between the precise interactions of effector pairs and their resulting modes of epigenetic memory.

Discussion

In this work, we devise a new platform technology called COMBINE for systematic, high-throughput functional screening of domain pairs. Importantly, COMBINE overcomes the length limitations and length-based biases of previous screening methodologies[27,28,35] to enable the characterization of large protein domains and beyond, which we demonstrate by testing combinatorial domain candidates up to 2,094 amino acids in length.

Applying COMBINE to epigenetic regulation of gene expression, we test over 50,000 pairs of epigenetic reader, recruiter, writer, and eraser domains across two libraries to understand emergent properties of combinatorial domain interactions that illuminate new biology and provide a rich ground for future epigenome editing tool development. In particular, our systematic analysis allowed us to capture broad, class-level trends of epigenetic effector activity, discover new and unexpected synergistic or antagonistic domain interactions, and quantitatively understand the contribution of individual domains and domain pairs to the modulation of target gene expression. Importantly, we establish our screen results are quantitative and generalizable across 5 endogenous genes through extensive secondary validation. We highlight new domain combinations that may prove useful for next-generation epigenome editing tools, including the pairing of the ZNF10 KRAB domain with the SAM domain from L3MBTL3 which improved target gene silencing by up to 34-fold in challenging, dose-limiting conditions. This robust activity enabled the substantial improvement of an aptamer-based bidirectional CRISPR perturbation setup[60,61], in which one target gene is silenced while another is activated using an orthogonal guide RNA-mediated effector recruitment strategy.

535 The inducible nature of the COMBINE platform allowed us to interrogate the durable effects of
536 domain pairs on target gene transcription following inducer washout. From this long-term
537 analysis, DNA methylation was nominated as the key modification driving heritable epigenetic
538 regulation. Expanding beyond previously observed epigenetic silencing memory[11,12], we also
539 observed domain combinations that elicited long-term graded target gene repression of
540 approximately 40%, or long-term gene activation of 30-40% – both of which were sustained for
541 at least 50 days. Importantly, the latter example establishes the ability of TET1 pairs to initiate
542 heritable gene activation from baseline expression levels and emphasizes the utility of our
543 combinatorial screening approach to identify unexpected pairings that greatly enhance the
544 potency and durability of this effect. We anticipate that these new epigenetic memory effectors
545 will expand the toolbox of long-term expression modulation technologies, complementary to
546 existing approaches such as CRISPRoff[12].
547
548 Our rich dataset quantifying the transcriptional output induced by over 50,000 epigenetic
549 effector pairs provides a broad resource for the epigenetics community to explore new
550 mechanistic hypotheses and pursue new biotechnological tools. Further, the COMBINE platform
551 is generalizable to many cell types due to its lentiviral delivery and is applicable beyond
552 epigenetics to study many outstanding questions in combinatorial biology. The ability to
553 systematically evaluate the functional interplay between entities–whether that includes DNA
554 elements, RNA species, protein domains, or entire proteins–will unlock a sophisticated
555 understanding of interactions in biology, where nothing acts in isolation.
556

Figures

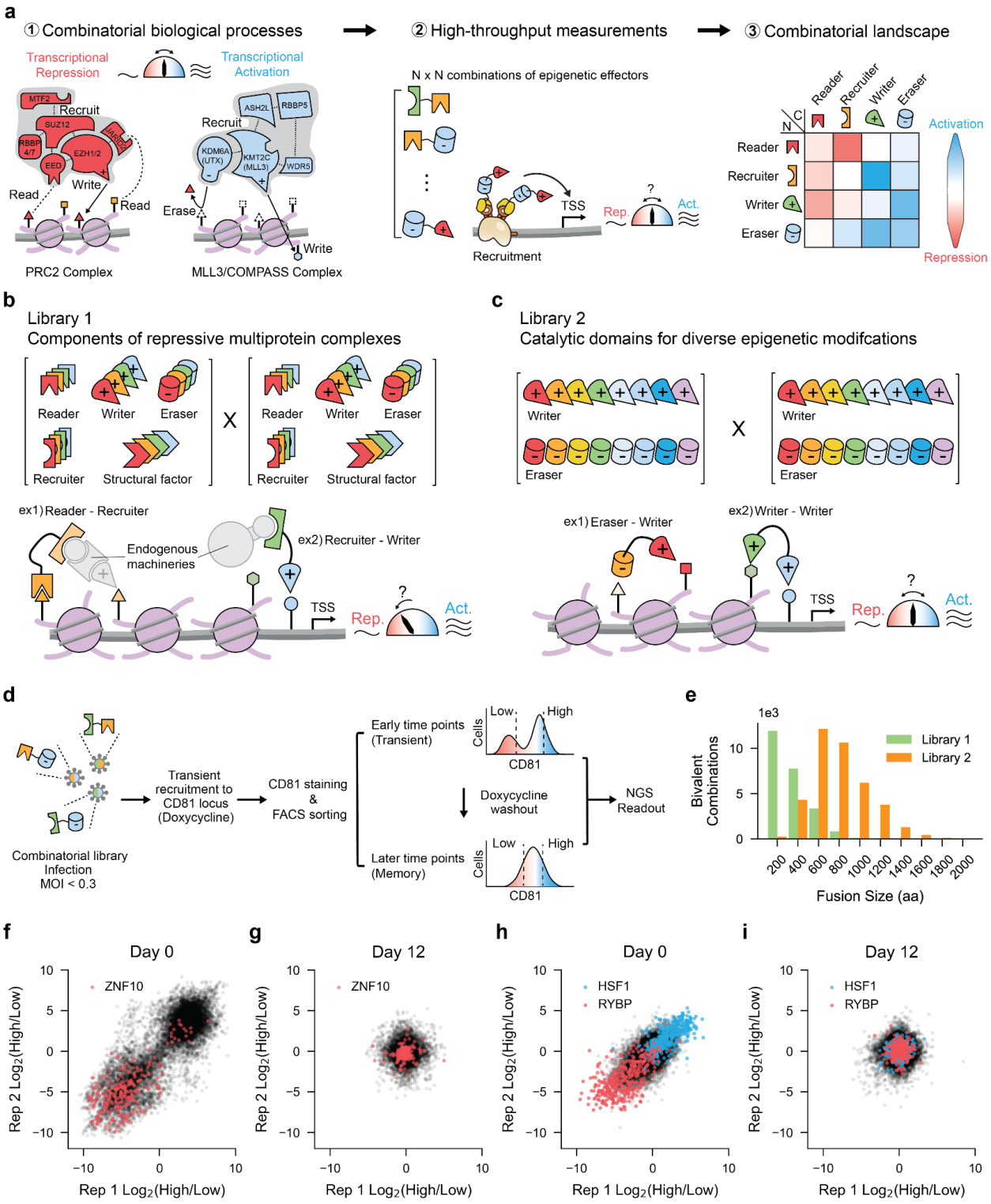
a
① Combinatorial biological processes
② High-throughput measurements
③ Combinatorial landscape
Transcriptional Repression
Transcriptional Activation
MTF2
Recruit
SUZ12
RBBP 4/7
EZH1/2
EED
JARID2
Read
Write
Read
PRC2 Complex
ASH2L
RBBP5
Recruit
KDM6A (UTX)
KMT2C (MLL3)
WDR5
Erase
Write
MLL3/COMPASS Complex
N x N combinations of epigenetic effectors
TSS
Rep.
Act.
Recruitment
Reader
Recruiter
Writer
Eraser
Activation
Repression
b
Library 1
Components of repressive multiprotein complexes
Reader
Writer
Eraser
Recruiter
Structural factor
X
ex1) Reader - Recruiter
Endogenous machineries
ex2) Recruiter - Writer
TSS
Rep.
Act.
c
Library 2
Catalytic domains for diverse epigenetic modifcations
Writer
Eraser
X
ex1) Eraser - Writer
ex2) Writer - Writer
TSS
Rep.
Act.
d
Combinatorial library Infection MOI < 0.3
Transient recruitment to CD81 locus (Doxycycline)
CD81 staining & FACS sorting
Early time points (Transient)
Low
High
Cells
CD81
Doxycycline washout
Later time points (Memory)
NGS Readout
e
1e3
Bivalent Combinations
Library 1
Library 2
Fusion Size (aa)
f
Day 0
ZNF10
Rep 2 Log2(High/Low)
Rep 1 Log2(High/Low)
g
Day 12
ZNF10
h
Day 0
HSF1
RYBP
i
Day 12
HSF1
RYBP

559 **Figure 1. COMBINE discovers novel epigenetic effector pairs that regulate**
560 **endogenous human transcription.**
561 (**a**) Conceptual framework for interrogating combinatorial biological processes through HTS of
562 an N x N combinatorial domain library. Schematics of representative multi-protein complexes,
563 including the Polycomb repressive complex 2 (PRC2) and the activating MLL3/COMPASS
564 complex, are shown. N x N combinatorial domains are recruited to the endogenous target gene
565 loci by a dCas9/MS2 system. Subpopulations of cells are enriched based on the target gene
566 expression level in a high-throughput manner. Following the NGS readout, the combinatorial
567 landscape of transcriptional perturbation is analyzed.
568 (**b**) Schematic of Library 1 composed of epigenetic readers, recruiters, structural factors, and
569 writers/erasers curated from diverse multiprotein complexes with an established ability to
570 mediate transcriptional repression. Two examples of possible domain pairs from Library 1 are
571 shown. A full list of members is available in **Supplementary Table 1**.
572 (**c**) Schematic of the composition of Library 2 including direct writers and erasers of diverse
573 epigenetic modifications, curated agnostic of their known effect on transcription. Two examples
574 of bivalent domain candidates from Library 2 are shown. A full list of members is available in
575 **Supplementary Table 2**.
576 (**d**) Experimental procedure for the combinatorial HTS of epigenetic effector pairs. Combinatorial
577 domain candidates are recruited to the endogenous CD81 locus for 5-6 days with the addition of
578 doxycycline. After staining with anti-CD81 antibody, cells are sorted into two bins (High and
579 Low) based on the CD81 expression level. NGS is performed to measure the enrichment of
580 bivalent domain candidates within sorted populations. Multiple timepoints are taken following the
581 doxycycline removal – Day 0, Day 6, and Day 12 for Library 1 and Day 0 and Day 12 for Library
582 2. For more detailed descriptions, refer to methods and **Supplementary Figs. 5** and **6**.
583 (**e**) Theoretical size distribution of bivalent domain candidates from Library 1 and 2 assuming
584 uniform coverage.
585 (**f**) Scatter plot of enrichment scores from Library 1 at Day 0. Effectors containing the repressive
586 ZNF10 KRAB domain are highlighted in red.
587 (**g**) Scatter plot of enrichment scores from Library 1 at Day 12. Effectors containing the
588 repressive ZNF10 KRAB domain are highlighted in red.
589 (**h**) Scatter plot of enrichment scores from Library 2 at Day 0. Effectors containing the repressive
590 RYBP domain are highlighted in red. Effectors containing the HSF1 activator are highlighted in
591 blue.
592 (**i**) Scatter plot of enrichment scores from Library 2 at Day 12. Effectors containing the
593 repressive RYBP domain are highlighted in red. Effectors containing the HSF1 activator are
594 highlighted in blue.
595

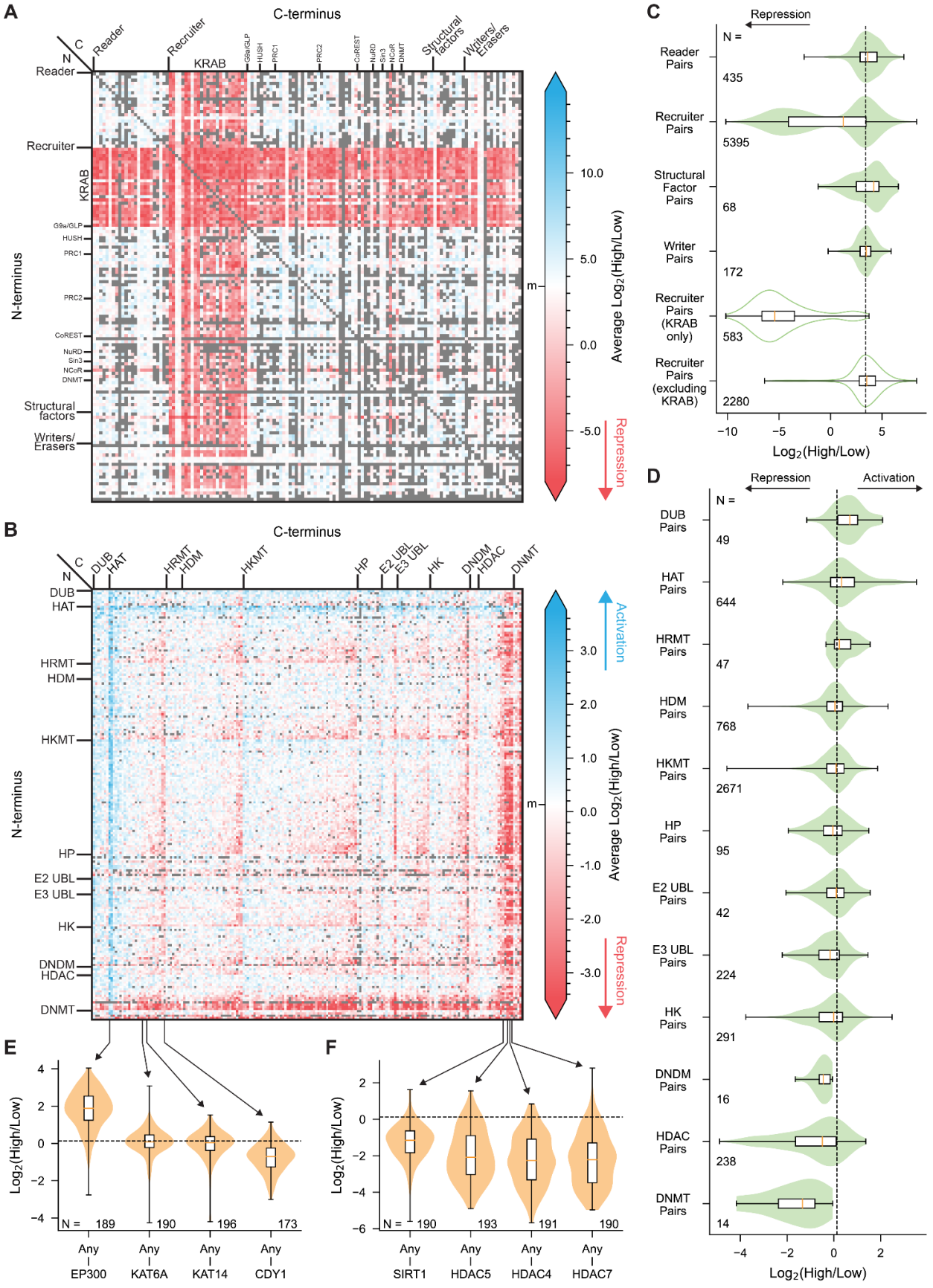
A
C-terminus
N-terminus
Reader
Recruiter
KRAB
G9a/GLP
HUSH
PRC1
PRC2
CoREST
NuRD
Sin3
NCoR
DNMT
Structural factors
Writers/ Erasers
Average Log2(High/Low)
Repression
B
DUB
HAT
HRMT
HDM
HKMT
HP
E2 UBL
E3 UBL
HK
DNDM
HDAC
Activation
C
Repression
N =
Reader Pairs
435
Recruiter Pairs
5395
Structural Factor Pairs
68
Writer Pairs
172
Recruiter Pairs (KRAB only)
583
Recruiter Pairs (excluding KRAB)
2280
Log2(High/Low)
D
Activation
DUB Pairs
49
HAT Pairs
644
HRMT Pairs
47
HDM Pairs
768
HKMT Pairs
2671
HP Pairs
95
E2 UBL Pairs
42
E3 UBL Pairs
224
HK Pairs
291
DNDM Pairs
16
HDAC Pairs
238
DNMT Pairs
14
E
N = 189 190 196 173
Any EP300
Any KAT6A
Any KAT14
Any CDY1
F
N = 190 193 191 190
Any SIRT1
Any HDAC5
Any HDAC4
Any HDAC7

596

Figure 2. Epigenetic pairs generate a rich combinatorial landscape of transient gene expression outcomes.

(**a**) Heatmap of enrichment scores generated from Library 1 at Day 0. Average Log_2(High/Low) enrichment scores across both replicates are plotted. Color scale is centered at the mode of the enrichment score distribution, indicated by the “m” tick. For this repressor-focused library, lower log_2 scores indicate stronger repression. Dropouts are indicated in gray.

(**b**) Heatmap of enrichment scores generated from Library 2 at Day 0. Average Log_2(High/Low) enrichment scores across both replicates are plotted. Color scale is centered at the mode of the enrichment score distribution, indicated by the “m” tick. For this library composed of putative repressors and activators, lower scores indicate more repression and higher scores indicate more activation. Histone deubiquitinase (DUB), histone acetyltransferase (HAT), histone arginine methyltransferase (HRMT), histone demethylase (HDM), histone lysine methyltransferase (HKMT), histone phosphatase (HP), E2 ubiquitin ligases (E2 UBL), E3 ubiquitin ligases (E3 UBL), histone kinase (HK), DNA demethylation machinery (DNDM), histone deacetylase (HDAC), and DNA methyltransferase (DNMT).

(**c**) Violin plots of all possible bivalent combinations within the same classes from Library 1. A breakdown of the recruiter class into KRAB and non-KRAB pairs is also shown (not shaded). The orange bar represents the median. Box spans quartile 1 to quartile 3. Whiskers extend to minimum and maximum. Number of combinations per class is indicated. The dashed line indicates the distribution mode of all pairs.

(**d**) Violin plots of all possible bivalent combinations within the same classes from Library 2. The orange bar represents the median. Box spans quartile 1 to quartile 3. Whiskers extend to minimum and maximum. Number of combinations per class is indicated. The dashed line indicates the distribution mode of all pairs.

(**e**) Violin plots of all possible bivalent combinations with the specified HAT effectors on the C-terminus. The orange bar represents the median. Box spans quartile 1 to quartile 3. Whiskers extend to minimum and maximum. Number of combinations per effector is indicated. The dashed line indicates the distribution mode of all pairs.

(**f**) Violin plots of all possible bivalent combinations with the specified HDAC effectors on the C-terminus. The orange bar represents the median. Box spans quartile 1 to quartile 3. Whiskers extend to minimum and maximum. Number of combinations per effector is indicated. The dashed line indicates the distribution mode of all pairs.

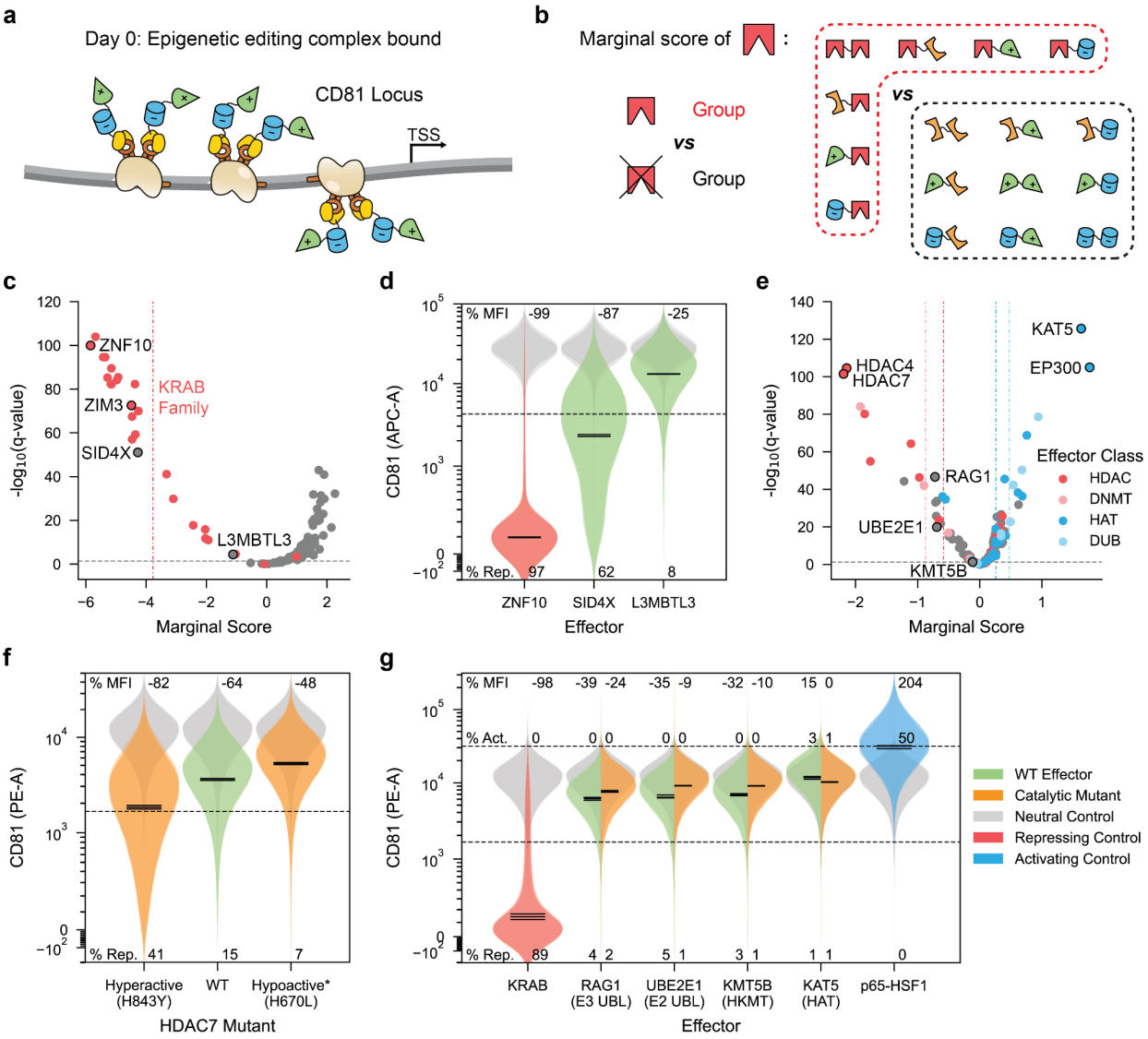

Figure 3. Marginal effector analysis reveals how individual domains perturb transcription across partners.

(**a**) Schematic of the dCas9/MS2 epigenetic editing complex bound at CD81 locus. Complex expression is induced by the addition of doxycycline and is recruited to the CD81 loci for 5-6 days prior to screen readout.

(**b**) Concept of marginal effector analysis. For a given effector, the marginal score is calculated as the difference in mean $\log_2$(High/Low) between all pairs containing the effector versus not containing the effector. Q-values were calculated as FDR-corrected p-values from Welsh's t-test.

(**c**) Volcano plot of marginal scores from Library 1 at Day 0. KRAB family members are highlighted in red. Vertical dashed line indicates the average marginal score across the KRAB family. Horizontal dashed line indicates q-value of 0.05.

(**d**) Violin plots of CD81 expression after expression of individual effectors from Library 1 in individual validation (3 days post nucleofection of effector encoding plasmids). Mock transfection of pUC19 colored in gray. 2 independent replicates illustrated as translucent

646 overlays. The geometric means of each replicate are shown as solid black lines. Dashed line
647 indicates repression gate at the 1st percentile of the pUC19 condition. The average percentages
648 of repressed cells in each condition are indicated. The average percent changes in CD81 mean
649 fluorescence intensity (MFI) versus pUC19 for each condition are indicated.
650 (**e**) Volcano plot of marginal scores from Library 2 at Day 0. Effectors from HDAC, DNMT, HAT,
651 and DUB classes are highlighted in red, pink, blue, and sky blue respectively. Vertical dashed
652 lines indicate average marginal score for each respective colored class. Horizontal dashed line
653 indicates q-value of 0.05.
654 (**f**) Violin plots of CD81 expression after expression of the HDAC7 deacetylase domain and its
655 mutants in individual validation (5 days post nucleofection and doxycycline induction). WT
656 HDAC7 is colored green. Mutants are colored orange. MCP-DMD neutral condition is colored in
657 gray. 3 independent replicates are illustrated as translucent overlays. The geometric means of
658 each replicate are shown as solid black lines. Dashed line indicates repression gate at the 1st
659 percentile of the neutral condition. The average percentages of repressed cells in each
660 condition are indicated. The average percent changes in CD81 MFI versus DMD for each
661 condition are indicated. *proposed mutant inferred from HDAC4.
662 (**g**) Violin plots of CD81 expression after expression of individual effectors from Library 2 in
663 individual validation (5 days post nucleofection and doxycycline induction). WT effectors are
664 colored green. Catalytic mutants are colored orange. Repressing and activating controls are
665 colored red and blue respectively. MCP-DMD neutral condition is colored gray. 3 independent
666 replicates are illustrated as translucent overlays. The geometric means of each replicate are
667 shown as solid black lines. Dashed lines indicate repression and activation gate at the 1st and
668 99th percentile of neutral condition. The average percentages of repressed and activated cells
669 in each condition are indicated. The average percent changes in CD81 MFI versus the neutral
670 DMD domain for each condition are indicated.
671

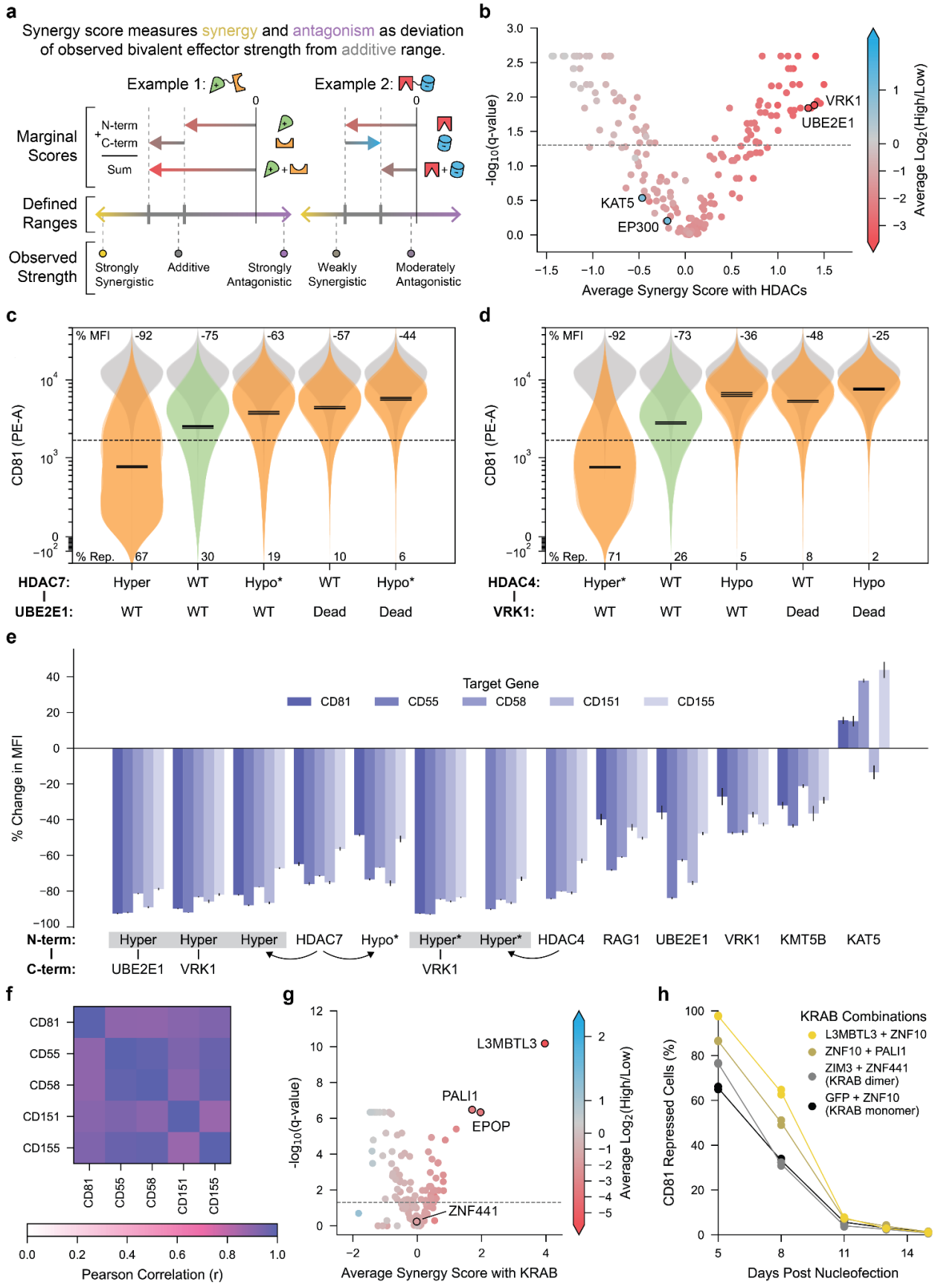
a
Synergy score measures synergy and antagonism as deviation of observed bivalent effector strength from additive range.
Example 1:
Example 2:
Marginal Scores
N-term
C-term
Sum
Defined Ranges
Observed Strength
Strongly Synergistic
Additive
Strongly Antagonistic
Weakly Synergistic
Moderately Antagonistic
b
-log10(q-value)
Average Synergy Score with HDACs
Average Log2(High/Low)
VRK1
UBE2E1
KAT5
EP300
c
% MFI
% Rep.
CD81 (PE-A)
HDAC7:
UBE2E1:
Hyper
WT
Hypo*
Dead
d
HDAC4:
VRK1:
Hyper*
Hypo
e
Target Gene
CD81
CD55
CD58
CD151
CD155
% Change in MFI
N-term:
C-term:
HDAC7
HDAC4
RAG1
UBE2E1
VRK1
KMT5B
KAT5
f
Pearson Correlation (r)
g
L3MBTL3
PALI1
EPOP
ZNF441
Average Synergy Score with KRAB
h
KRAB Combinations
L3MBTL3 + ZNF10
ZNF10 + PALI1
ZIM3 + ZNF441 (KRAB dimer)
GFP + ZNF10 (KRAB monomer)
CD81 Repressed Cells (%)
Days Post Nucleofection

672

673 **Figure 4. COMBINE uncovers diverse modes of epigenetic interactions.**
674 (**a**) Concept of synergy score calculation to quantify synergy and antagonism. Marginal scores
675 of each individual effector are used to calculate an additive range for each bivalent combination.
676 The lower bound of the additive range is defined as the minimum of the N-terminal effector's
677 marginal score, the C-terminal effector's marginal score, and the sum of the marginal scores.
678 The upper bound is defined as either the sum of the marginal scores or the minimum of the N-
679 terminal and C-terminal marginal scores (whichever is higher). The magnitude of the synergy
680 score represents how far outside the additive range the mean-centered observed bivalent
681 enrichment score falls. Synergy is indicated by positive synergy scores, while antagonism is
682 indicated by negative synergy scores. Two example cases illustrate the calculation of synergy
683 scores. Library 1 synergy scores are all calculated in the repression direction. Library 2 synergy
684 scores are calculated both in the activation and repression direction depending on whether the
685 sum of marginal scores is positive or negative, respectively.
686 (**b**) Volcano plot of average synergy scores with HDAC family from Library 2 on Day 0. Effectors
687 are colored based on the average $\log_2$(High/Low) enrichment scores across all combinations of
688 the given effector with significant HDAC repressors. Q-values were calculated as FDR-corrected
689 p-values from a one-sample Wilcoxon test. Horizontal dashed line indicates q-value of 0.05.
690 (**c**) Violin plots of CD81 expression at 5 days after nucleofection and induction of the HDAC7 +
691 UBE2E1 combination and its mutants. WT domains are colored green. Mutant combinations are
692 colored orange. MCP-DMD neutral condition is colored in gray. 3 independent replicates are
693 illustrated as translucent overlays. The geometric means of each replicate are shown as solid
694 black lines. Dashed line indicates repression gate at the 1st percentile of neutral condition. The
695 average percentages of repressed cells in each condition are indicated. The average percent
696 changes in CD81 MFI versus DMD for each condition are indicated. *proposed mutant inferred
697 from homology to HDAC4.
698 (**d**) Violin plots of CD81 expression at 5 days after nucleofection and induction of HDAC4 +
699 VRK1 and enzymatic mutants. WT domains are colored in green. Mutant combinations are
700 colored orange. MCP-DMD neutral condition colored gray. 3 independent replicates are
701 illustrated as translucent overlays. The geometric means of each replicate are shown as solid
702 black lines. Dashed line indicates repression gate at the 1st percentile of neutral condition. The
703 average percentages of repressed cells in each condition are indicated. The average percent
704 changes in CD81 MFI versus DMD for each condition are indicated. *proposed mutant inferred
705 from HDAC7.
706 (**e**) Percent change in MFI relative to the neutral DMD control following dual nucleofection of
707 plasmids encoding key transient effectors from Library 2 and 3X guide arrays targeting CD55,
708 CD58, CD151, and CD155. CD81 percent MFIs are from single plasmid nucleofection into Tet-
709 On dCas9 cell line with preinstalled 3X CD81 guide array. The dCas9/MS2 complex was
710 induced by doxycycline for 5 days. Error bars represent the standard deviation between 3
711 independent replicates. *, proposed mutant inferred from homology. Lack of C-terminal effector
712 indicates that the effector was tested monovalently. Arrows point from WT effector to mutant
713 form of the same effector. Gray boxes indicate the same effector. Additional detailed data are
714 shown in **Supplementary Fig. 16**.

715 (**f**) Heatmap of Pearson correlations of percent change in MFI versus the neutral DMD control
716 between each gene tested. Datasets consist of the 13 effectors shown in (**e**). Additional detailed
717 data are shown in **Supplementary Fig. 17**.
718 (**g**) Volcano plot of average synergy scores with KRAB family from Library 1 on Day 6. Effectors
719 are colored based on the average $\log_2$(High/Low) enrichment scores across all combinations of
720 the given effector with significant KRAB repressors. Q-values were calculated as FDR-corrected
721 p-values from a one-sample Wilcoxon test. Horizontal dashed line indicates q-value of 0.05.
722 (**h**) Timecourse of CD81 repression following nucleofection of plasmids encoding KRAB
723 combinations (n=2 independent replicates).
724

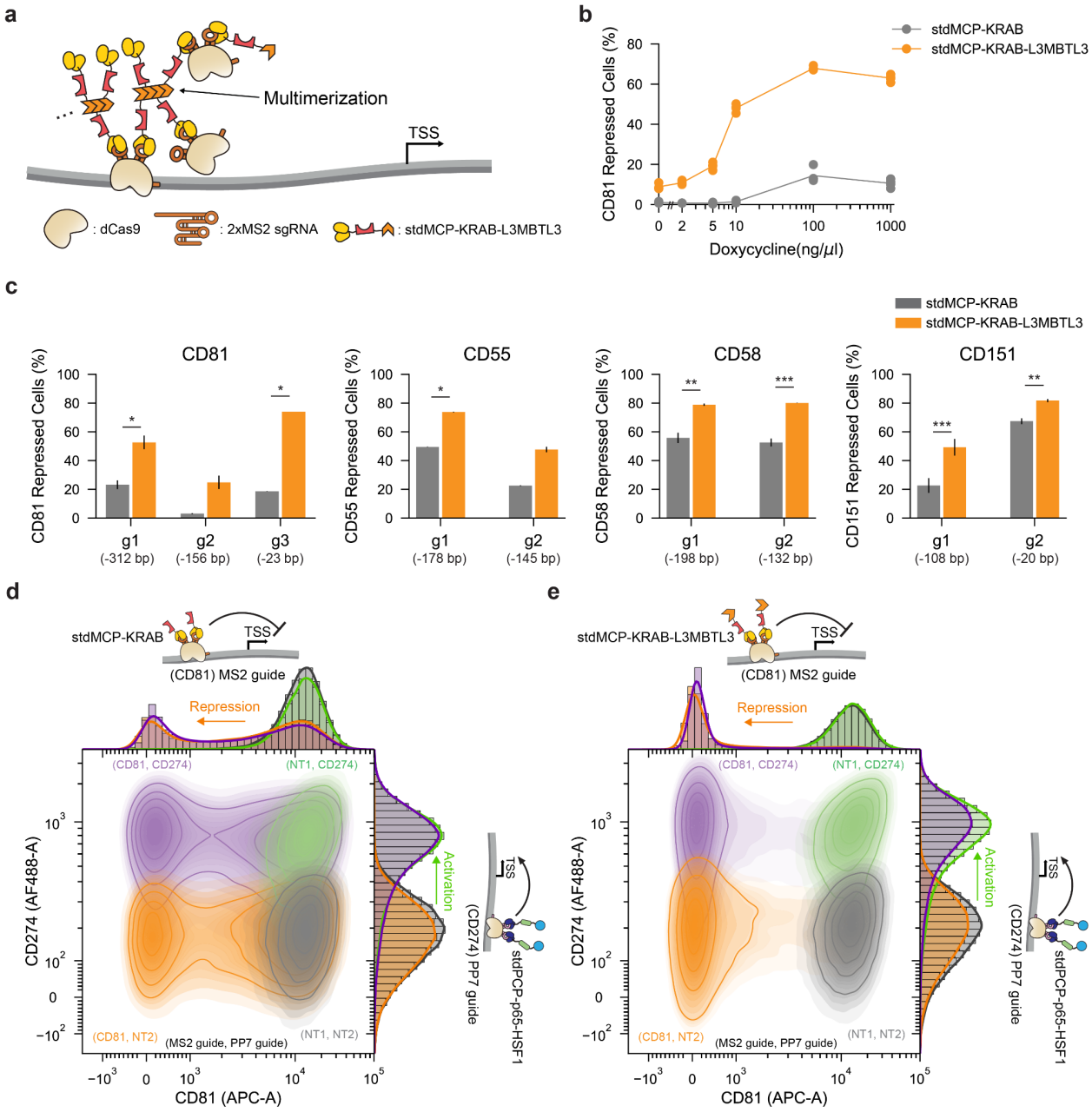

Figure 5. A combination of KRAB and L3MBTL3 enables robust and bidirectional transcriptional perturbation.

(**a**) Illustration of hypothetical clustering of the dCas9/MS2 complex due to the multimerization property of the SAM domain of L3MBTL3.

(**b**) Doxycycline response curve of CD81 repression by stdMCP-KRAB and stdMCP-KRAB-L3MBTL3 4 days after doxycycline induction (n = 4 biological replicates). KRAB domain is from ZNF10.

(**c**) Target gene repression 5 days following lentiviral transduction with sgRNA and doxycycline induction of the effector components (n ≥ 2 biological replicates). Distance between the sgRNA

target site and the TSS is indicated in parentheses. Error bars indicate the standard deviation of 4 biological replicates. * p-value < 0.05, ** p-value < 0.01, *** p-value < 0.001; two-tailed t-test.

(**d**) 2D-contour plot and kernel density estimate (KDE) plots of populations transduced with dual MS2/PP7 sgRNAs. stdMCP-KRAB was recruited for CD81 gene repression and stdPCP-p65-HSF1 was recruited for the activation of CD274 gene expression. CD81/CD274 expression profiles were measured 5 days following lentiviral transduction with sgRNAs and doxycycline induction of the effector components. Genes within parentheses indicate the target genes for MS2 and PP7 sgRNAs, respectively. For example, (CD81, NT1) denotes that the CD81 gene is targeted by the MS2 sgRNA, while NT1 (non-target 1) is a control sgRNA used with PP7.

(**e**) 2D-contour plot and kernel density estimate (KDE) plots of populations infected with dual MS2/PP7 sgRNAs. stdMCP-KRAB-L3MBTL3 was recruited for CD81 gene repression and stdPCP-p65-HSF1 was recruited for the activation of CD274 gene expression. CD81/CD274 expression profiles were measured 5 days following lentiviral transduction with sgRNAs and doxycycline induction of the effector components. Genes within parentheses indicate the target genes for MS2 and PP7 sgRNAs, respectively. For example, (CD81, NT1) denotes that the CD81 gene is targeted by the MS2 sgRNA, while NT1 (non-target 1) is a control sgRNA used with PP7.

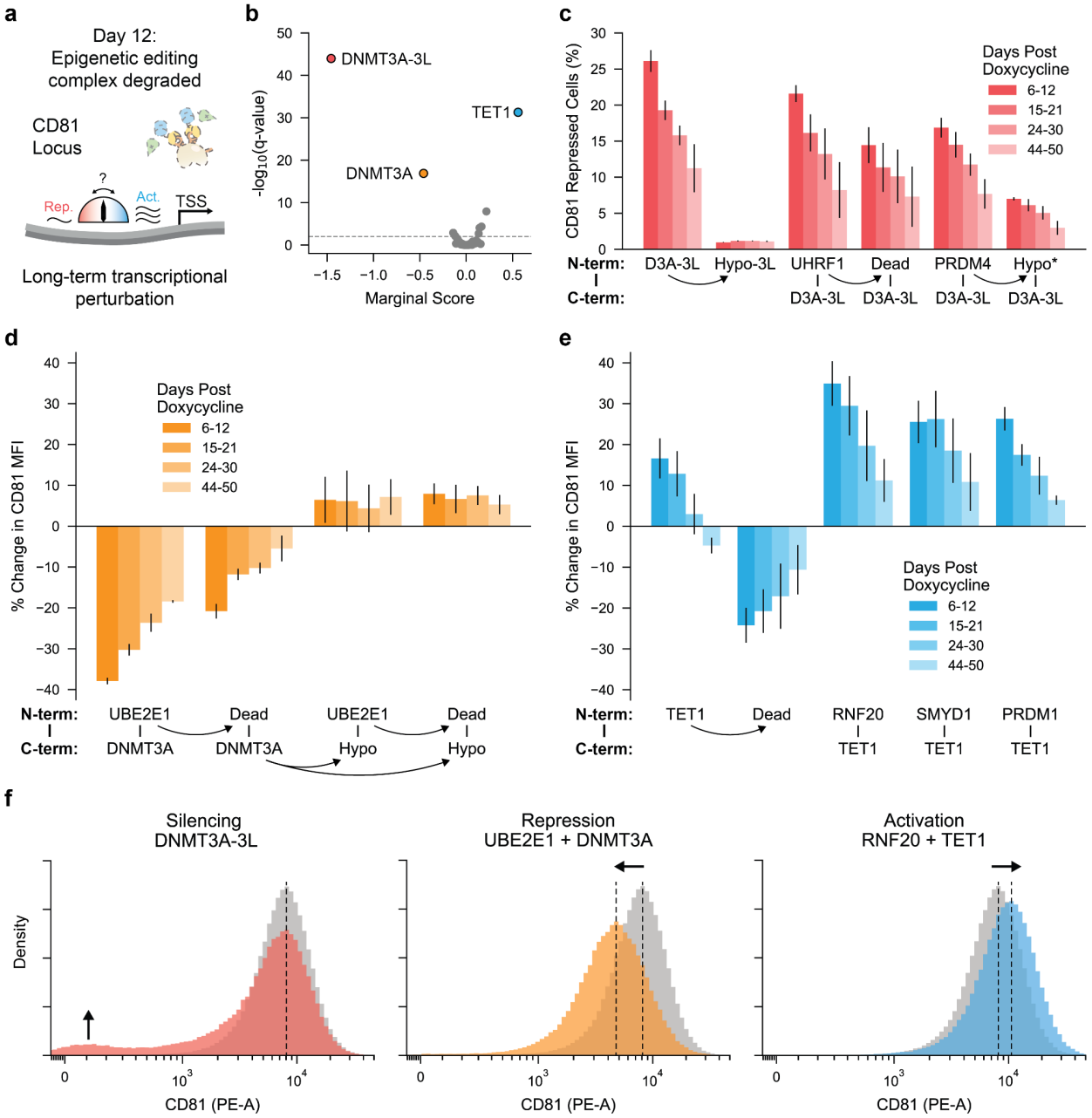

Figure 6. DNA methylation writers and erasers are essential for the memory of silencing, repression, and activation of gene expression.

(**a**) Schematic showing loss of the dCas9/MS2 epigenetic editing complex 12 days post-withdrawal of doxycycline. CD81 expression perturbations rely on sustained epigenetic modifications.

(**b**) Volcano plot of marginal scores from Library 2 on Day 12. Horizontal dashed line indicates q-value of 0.05.

(**c**) Timecourse of CD81 repression following nucleofection of plasmids encoding DNMT3A-3L combinations and induction of the dCas9/MS2 complex by doxycycline treatment for 5 days. Day 0 indicates the day of doxycycline washout. Each bar represents 3 timepoints collected within the specified days. The bar heights represent the average perturbation across the

765 timepoints, and the error bars represent the standard deviation between 3 independent
766 replicates. *proposed mutant inferred from PRDM7. Lack of C-terminal effector indicates that
767 the effector was tested monovalently. Arrows point from WT effector to mutant form of the same
768 effector. Additional detailed data are shown in **Supplementary Fig. 21**.
769 (**d**) Timecourse of CD81 MFI relative to the neutral DMD control following nucleofection of
770 plasmids encoding UBE2E1 + DNMT3A combinations and induction of the dCas9/MS2 complex
771 by doxycycline for 5 days. Day 0 indicates the day of doxycycline washout. Each bar represents
772 3 timepoints collected within the specified days. The bar heights represent the average
773 perturbation across the timepoints, and the error bars represent the standard deviation between
774 3 independent replicates. Arrows point from WT effector to mutant form of the same effector.
775 Additional detailed data are shown in **Supplementary Fig. 22**.
776 (**e**) Timecourse of CD81 MFI relative to the neutral DMD control following nucleofection of
777 plasmids encoding TET1 combinations and induction of the dCas9/MS2 complex by doxycycline
778 for 5 days. Day 0 indicates the day of doxycycline washout. Each bar represents 3 timepoints
779 collected within the specified days. The bar heights represent the average perturbation across
780 the timepoints, and the error bars represent the standard deviation between 3 independent
781 replicates. Lack of C-terminal effector indicates that the effector was tested monovalently.
782 Arrows point from WT effector to mutant form of the same effector. Additional detailed data are
783 shown in **Supplementary Figs. 23** and **24**.
784 (**f**) Representative CD81 expression profiles illustrating three types of gene expression memory.
785 CD81 expression levels were measured 12 days after doxycycline washout following 5 days of
786 doxycycline induction.
787

Methods

Cell lines and cell culture

All experiments in this study were carried out in K562 cells (ATCC, CCL-243, female). Cells were cultured in a humidified incubator at 37°C and 5% CO_2, in RPMI 1640 (Gibco, 61870036) media supplemented with 10% fetal bovine serum (FBS) (Gibco, 26140095) and 1% penicillin-streptomycin (Gibco, 15140122). For Library 1 lentivirus generation, 293FT (Thermo Fisher Scientific) or Lenti-X 293T (Takara) were cultured in a humidified incubator at 37°C and 5% CO_2, in DMEM (Gibco, 10566016) media supplemented with 10% fetal bovine serum (FBS) (Gibco, 26140095) and 1% penicillin-streptomycin (Gibco, 15140122). For Library 2 lentivirus generation, viral production cells (Gibco, A35347) were cultured according to the manufacturer's instructions.

Guide design and cloning

CRISPRa guides were generated using CHOPCHOP for the CD81, CD55, CD58, CD151, and CD155 genes, and three were selected to tile each promoter region from -500-0 to the TSS (**Supplementary Table 8**, Guides)[79]. A tiered golden gate approach was developed to assemble a 3X guide array and to easily insert this array into a landing pad PiggyBac vector, which was cloned in part using the EMMA toolkit[80], between divergent expression cassettes pTRE3G-dCas9-tagBFP and pEF1a-BlastR-P2A-rTA3 (**Supplementary Table 8**, Plasmids, pMH224). Briefly, the three guides were cloned separately via BsmBI golden gate into three distinct guide expression plasmids containing different golden gate overhangs around the guide cassette (**Supplementary Table 8**, Plasmids, pMH213-pMH215). The guide scaffold contained MS2 aptamers in stemloop two and the tetraloop and was sourced from recent optimization[32]. These individual guide plasmids were then assembled via BsaI golden gate into a RFP dropout landing pad containing pSV40-mCherry for mammalian expression (**Supplementary Table 8**, Plasmids, pMH222). Guides were arranged in the 3X array such that the closest guide to the TSS was placed first, followed by the middle guide and then the furthest guide. The CD81 3X guide array plasmid was used directly for guide nucleofection in screening of Library 1 (**Supplementary Table 8**, Plasmids, pMH228). This 3X array was further assembled into pMH224 via a final BsmBI golden gate for PiggyBac insertion and constitutive guide expression, which was used for screening Library 2 (**Supplementary Table 8**, Plasmids, pMH260). Additional sgRNAs targeting before the TSS of CD55, CD58, CD151, and CD274 were generated using CHOPCHOP (**Supplementary Table 8**, Guides)[79]. CD55, CD58, and CD151 guides were inserted into a lentiviral vector containing the recently optimized MS2 guide scaffold[32] driven by human U6 promoter and SV40 promoter driven-mCherry marker. For bidirectional perturbation experiments, the CD274 guide (**Supplementary Table 8**, Guides) was cloned into the human U6-driven PP7 guide scaffold within a lentiviral vector, where both MS2 sgRNA and PP7 sgRNA are expressed from distinct mouse and human U6 promoters, respectively.

PB Tet-On dCas9 cell line generation

To generate Tet-On dCas9 K562 cell lines expressing pTRE3G-dCas9-tagBFP, pEF1a-BlastR-P2A-rTA3 with or without the 3X CD81 guide array, K562 cells were nucleofected with

600 ng of pMH224 or pMH260 and 200 ng of a separate PiggyBac transposase plasmid using SF Cell Line 96-well Nucleofector kit and protocol (Lonza, V4SC-2096) (**Supplementary Table 8**, Plasmids). Two days following nucleofection, a 10-day selection began with 10 µg/mL blasticidin (Gibco, A1113903). After selection, cells were expanded and assessed for BFP induction in response to 1 µg/mL doxycycline. This Tet-On dCas9 K562 (with CD81 guide array) cell line was used for Library 2 HTS and Library 1 validation experiments, while this Tet-On dCas9 K562 (without CD81 guide array) was used for validation of Library 2 effectors on additional genes.

An additional Tet-On dCas9 K562 (without CD81 guide array) cell line was generated that expresses pTREtight-dCas9 and pEF1a-BlastR-P2A-rTA3. K562 cells were co-transfected with Piggybac plasmid encoding both pTREtight-dCas9 and pEF1a-BlastR-P2A-rTA3 (without transposases) and PiggyBac transposase plasmid using Lipofectamine 2000 (Invitrogen). Two days following transfection, 20 µg/mL blasticidin (Gibco, A1113903) selection was performed for at least 10 days. This Tet-On dCas9 K562 (without CD81 guide array) cell line was used for Library 1 HTS.

Library 1 design and cloning

A literature review was conducted to cover critical components of the key repressive epigenetic multiprotein complexes and structural factors for chromatin organization. The majority of library members were selected based on previous arrayed studies employing truncation-based co-immunoprecipitation experiments or luciferase assays, except for the few members from high-throughput studies[24]. Peptides shorter than 80 amino acids were expanded equally on either side to reach 80 amino acids in total. Start codons were removed as effectors were to be fused to the C-terminus of aptamer binding protein. Amino acid sequences were back-translated with mammalian species codon optimization and forbidding 3′ end 6-mer of both amplification primers motifs (GGTGTG and ATGGCC) by Geneious Prime. Second codon optimization was performed for human codon usage, removing several type IIS restriction enzyme sites (BbsI, BsaI, BsmBI, BspQI, BtgZI, and SapI) and constraining GC content to between 35% and 65% in every 50 nucleotides window by DNA chisel[81]. Forward amplification primer binding handle (TCCaGACCGTTCaGGTGTG adapted from previous study[24]), BsaI binding site (GGTCTCT), and overhang (GTCA) facilitating ‘Glutamic-acid (E) – Serine (S)’ peptide overhang for C-terminus of XTEN16 linker were appended to 5′ of the gene fragment (**Supplementary Fig. 2a**). Overhang (AGTG) for ‘Serine (S) – Glycine (G)’ peptide overhang at N-terminus of XTEN16 linker, BsaI binding site (CGAGACC), and reverse amplification primer binding handle (gGCCaTGCGGaATGGGTTA) were appended to 3′ of the gene fragment. Optimized golden gate assembly overhangs were selected based on a previous study[82]. A few BsmBI sites, BsaI sites, and 3′ end 6-mer of both amplification primers motifs (GGTGTG and ATGGCC) that were unintentionally generated by former procedures were manually modified by silent mutations. Finally, library members that did not pass the Gblock or Eblock complexity test were human codon-optimized by IDT webtool, and again BsmBI, BsaI sites, and 3′ end 6-mer of both amplification primers motifs were manually modified by silent mutations.

Double-stranded gene fragments were synthesized (IDT and Twist Biosciences) and then pooled manually without PCR amplifications to make a 20 nM solution with the molarity of each fragment increasing proportional to its length with a slope of 1. For example, we added

875 1.5-fold of the 450 bp gene fragment compared to the 300 bp gene fragment. The pooled library
876 was subcloned into KanR1_receiver (pCM001) and KanR2_reveiver (pCM002) plasmids by two
877 separate golden gate reactions. For a total volume of 40 µL golden gate reaction, we used 185
878 ng of KanR1 (pCM001) or KanR2 (pCM002) receiver plasmid, 10 µL of 20 nM pooled library for
879 ~2:1 molar ratio between backbone:insert, 2 µL of BsaI-HFv2 (NEB, 20000 U/mL), 2 µL of T4
880 DNA ligase (NEB, 400000 U/mL), and 4 µL of 10X T4 DNA ligase buffer (NEB). The
881 thermocycling protocol was 30 cycles of 5 min digestion at 37°C and 5 min ligation at 16°C,
882 followed by a final 5 min digestion at 37°C, 5 min heat inactivation at 60°C and an extra 20 min
883 heat inactivation at 70°C. The reactions were then purified with DNA Clean & Concentrator-5
884 (Zymo) and were eluted by 8 µL of nuclease-free water (Ambion). 1 µL of purified DNA was
885 transformed into 25 µL of Endura electrocompetent cells (Lucigen) following the manufacturer's
886 instructions with 2 mL of prewarmed recovery media. 2 mL of cells were plated onto a 245 mm x
887 245 mm plate, and serially diluted cells were plated onto 100 mm diameter plates for the
888 estimation of colony numbers. After overnight incubation at 30°C, colonies were collected, and
889 plasmid libraries were extracted with Maxiprep (Machery-Nagel). Colony coverage was at least
890 34000X for 155 library members.
891 For the final bivalent library construction, the LV_AmpR_backbone (pCM003) was
892 predigested with FastDigest Esp3I (Thermo Fisher Scientific) and gel extracted. For a total
893 volume of 100 µL golden gate reaction, we used 800 ng of predigested and gel-extracted
894 LV_AmpR_backbone (pCM003), 1000 ng of N-terminus effector (KanR1_recevier) library, 1000
895 ng of C-terminus effector (KanR2_receiver) library, 10 µL of FastDigest Esp3I (Thermo Fisher
896 Scientific), 5 µL of T4 DNA ligase (NEB, 400000 U/mL), and 10 µL of 10X T4 DNA ligase buffer
897 (NEB). The thermocycling protocol was initial 5 min digestion at 37°C, 30 cycles of 5 min
898 digestion at 37°C and 10 min ligation at 16°C, final 20 min ligation at 16°C, final 5 min digestion
899 at 37°C, and 20 min heat-inactivation at 75°C. The golden gate reaction was then isopropanol
900 precipitated into 10 µL of nuclease-free water (Ambion)[83]. Again, 1 µL of purified DNA was
901 transformed into 25 µL of Endura electrocompetent cells (Lucigen) following the manufacturer's
902 instructions with 2 mL of prewarmed recovery media. 2 mL of cells were plated onto a 245 mm x
903 245 mm plate and serially diluted cells were plated onto 100 mm diameter plates for the
904 estimation of colony numbers. After overnight (15 hours) incubation at 30°C, colonies were
905 collected, and plasmid pools were extracted with Maxiprep (Machery-Nagel). Colony coverage
906 for 1 bioassay plate was at least 1100X for 155^2 library members. Two separate maxi-prepped
907 DNA solutions from two bioassay plates were mixed to achieve at least 2200X colony coverage
908 of library members.
909
910 **High-throughput assay to measure transcriptional effects of Library 1**
911 Low passage 293FT cells (Invitrogen) or Lenti-X (Takara) 293T cells were grown in
912 DMEM (Invitrogen, 10566-016) supplemented with 10% FBS (Gibco) and 1% Penicillin-
913 Streptomycin (Gibco). For one T225 flask, 39.9 µL of 1 mg/mL PEI MAX (Polysciences) and 1
914 mL of DMEM were mixed by inversion and incubated at room temperature for 10 min. During
915 incubation, 5.6 µg of pMD2.G, 11.3 µg of psPAX2, and 22.7 µg of target plasmid or plasmid
916 library were added to new 1 mL of DMEM and were thoroughly mixed by vortexing. After
917 incubation, plasmids + DMEM mixture was added to PEI MAX + DMEM mixture followed by 30
918 sec vortexing. The final ~2 mL mixture of plasmids + PEI MAX + DMEM was incubated at room

919 temperature for 30 min. During incubation, 293FT or Lenti-X 293T cells were split by TrypLE
920 (Gibco) and 33.4 million cells were added to a standing T225 flask in 5 mL of fresh growth
921 media. After the 30 min incubation, plasmids + PEI MAX + DMEM mixture was added to the
922 flask, and the flask was gently mixed by swirling. The flask was incubated for 5 min in the
923 upright position. Following the 5 min incubation, fresh growth media was added up to 45 mL,
924 and cells were incubated at 37°C, 5% CO_2 overnight. The next day (Day 1), the media was
925 changed to 45 mL of fresh growth media and incubated for an additional 2 days, after which the
926 supernatant was collected and concentrated by Lenti-X concentrator (Takara) following the
927 manufacturer's protocol.
928 Upon infection of 40 million PB Tet-On dCas9 cells (without CD81 guide array) with 200
929 µL of lentivirus per replicate on Day -13, cells were cultured in growth media containing 1-2
930 µg/mL doxycycline (**Supplementary Fig. 5**). In parallel, 2 control cell lines (negative control: PB
931 Tet-On dCas9 cells without any effector & positive control: PB Tet-On dCas9 cells with LV-
932 pTRE3G-PuroR-T2A-stdMCP-eGFP-KRAB (ZNF10) preinstalled by lentiviral infection) started
933 doxycycline incubation as well. Doxycycline was replaced or added daily, maintaining the
934 concentration of 0.5-2 µg/mL to compensate for the short half of doxycycline in the media. 1 day
935 post-infection (Day -12), puromycin selection started with a 1 µg/mL concentration. To
936 simultaneously measure the lentiviral titer, subsets of cells were passaged to 96 well plates for
937 the viability assay. 3 days after the start of puromycin selection (Day -9), lentiviral titer was
938 measured by the CellTiter-Glo 2.0 Cell Viability Assay (Promega G9242) as previously
939 described[83]. Measured viability was 0.25-0.29 suggesting successful low MOI infection.
940 Puromycin selection was continued for an additional 3 days until Day -6. We observed an
941 increase in the percentage of live cells by trypan blue staining (Thermo Fisher Scientific) during
942 the additional 3 days of selection, suggesting the outgrowth of infected cells over debris from
943 dead cells.
944 After a total of 6 days of puromycin selection and outgrowth (Day -6), 39.2 million
945 surviving cells were mixed with 0.8 million positive control cells (LV-pTRE3G-PuroR-T2A-
946 stdMCP-eGFP-KRAB (ZNF10)) per replicate. On Day -6, mixed cells were nucleofected with the
947 CD81 targeting 3X guide array plasmid (pMH228). For each cuvette, 4 million cells were
948 nucleofected with 4.5 µg of pMH228 following the manufacturer's K562-specific protocol (4D X-
949 unit, FF-120 program, Lonza). For each replicate, 40 million cells were nucleofected by 10
950 cuvettes. 4 million positive control cells were also nucleofected by 1 cuvette. 3 days post-
951 nucleofection (Day -3), mCherry-positive cells were sorted. To reduce the variability generated
952 by sgRNA expression level, a population expressing moderate levels of mCherry was sorted
953 (**Supplementary Fig. 5b**). In total, ~9.7 million cells (~400X coverage) were sorted for each
954 replicate. 3 days post-sorting (Day 0), at least 11.5 million cells per replicate were frozen for
955 future FACS sorting. The remaining half of at least 11.5 million cells were centrifuged and
956 passaged to media without doxycycline to stop the expression of dCas9 and the stdMCP-
957 combinatorial effectors. Cells were continuously expanded until Day 6 in culture media without
958 doxycycline. On Day 6, 50 million cells were frozen for each replicate. Cells were again
959 continuously expanded until Day 12. On Day 12, 120 million cells were frozen for each replicate.
960 On the day of FACS, frozen cells from various timepoints (Day 0, 6, and 12) were
961 thawed briefly and washed twice with eBioscience Flow Cytometry Staining Buffer (Invitrogen).
962 APC Mouse Anti-Human CD81 antibody (Cat# 561958, BD Bioscience) was diluted 1:10 in 100

963 μL stain buffer per 0.1 million cells. Staining was performed on a 3D rotary mixer in a cold room
964 (4°C) for 1 hour. Cells were washed twice with stain buffer and sorted using a FACSAria Fusion
965 Special Order Research Product (BD Bioscience). mCherry-negative singlet populations were
966 separated into two populations based on CD81 level (**Supplementary Fig. 5c**). Sorted cells
967 were frozen at -80°C until genomic DNA extraction.
968 Genomic DNA (gDNA) was extracted using columns from the Quick-DNA Miniprep Plus
969 kit (Zymo Research) and reagents from the Quick-DNA Midiprep Plus kit (Zymo Research) with
970 the following modifications in the protocol. Cells were split into multiple columns if the number of
971 cells was larger than 3 million. Per 3 million cells, excess genomic lysis buffer (Beta-
972 Mercaptoethanol added) with a volume of 1.6 mL from the Quick-DNA Midiprep Plus kit (Zymo
973 Research) was used instead of BioFluid & Cell Buffer from the Quick-DNA Miniprep Plus kit
974 (Zymo Research). After the addition of 1.6 mL genomic lysis buffer to the cells, the mixture was
975 vortexed thoroughly. Cells were lysed in genomic lysis buffer for 1 hour at room temperature
976 with 3D rotation. Excess genomic lysis buffer ensured complete lysis of the cells, yielding a high
977 amount of extracted gDNA. Except for the described cell lysis step, we followed the
978 manufacturer's protocol for the Quick-DNA Miniprep Plus kit (Zymo Research).
979 Enriched combinatorial library members were PCR amplified from the gDNA using the
980 following conditions. For one 50 μL of the PCR reaction, 25 μL of 2X NEBNext HiFi (NEB), 1 μg
981 of gDNA, and a final concentration of 0.5 μM for each forward and reverse NGS primers
982 (**Supplementary Table 8**) were prepared and mixed on ice. One-step NGS primers were
983 designed to have 0~7 random spacer nucleotides to increase the base diversity during the initial
984 sequencing cycles[84]. The thermocycling protocol was 1 cycle of 98°C for 3 min, 27 cycles of
985 98°C for 10 sec, 64°C for 30 sec, 72°C for 75 sec, and final 1 cycle of 75°C for 2 min. After
986 thermocycling, PCR reactions were pooled and run through multiple lanes in 1.2% TBE gel.
987 Rectangular regions of the gel spanning from 800 bp ~ 2 kb were excised, and PCR products
988 were extracted using Monarch DNA Gel Extraction Kit (NEB). The gel-extracted library was
989 quantified by Nanodrop (Thermo Fisher Scientific), Qubit HS kit (Thermo Fisher Scientific),
990 Bioanalyzer (Agilent Technologies), and KAPA Library Quantification Kit (Roche). We noticed
991 approximate agreement in quantification between Qubit and Bioanalyzer while KAPA library
992 quantification exhibited the most discrepancy, potentially due to differences in the size between
993 our library and the standards provided by the kit. Based on the results of Qubit and Bioanalyzer,
994 the library was pooled with ~10% PhiX control (Illumina) and sequenced on a NextSeq2000
995 (Illumina) with 2 x 300 bp P2 kits (Illumina). In total, two 2 x 300 bp P2 kits were used. Libraries
996 from Day 0 and 6 were pooled together and sequenced with one kit, and the Day 12 library was
997 sequenced separately using the second kit.
998
999 **NGS analysis of bivalent domains from Library 1**
1000 To address the issue of lower R2 sequencing quality, which is occasionally observed
1001 during paired-end readout of long fragments[85], we implemented an approach of spreading ten
1002 15-mer short identifiers (IDs) across the entire 301 bp sequencing region. If any of the 10 IDs
1003 exactly matched the NGS read, the read was assigned to the corresponding domain. Unique 15
1004 mer IDs for identifying N- and C-terminal domains were generated by the following steps.

Step 1) From fasta files composed of expected 301 bp NGS reads for every domain (R1_Forward_P5_301cycles.fasta & R2_Reverse_P7_301cycles.fasta), all possible unique 15 mers were generated using UniqueKMER with the following commands[86].

```
$ uniquekmer -f R1_Forward_P5_301cycles.fasta -k 15 -o "kmercollection_R1"
$ uniquekmer -f R2_Reverse_P7_301cycles.fasta -k 15 -o "kmercollection_R2"
```

Step 2) If a 15 mer ID for one domain had a hamming distance of less than 2 with an ID from another domain, one of the IDs was deleted from the domain with a larger number of IDs by executing Library1_step2.py. Output files were numerically sorted using Seqkit with the following commands[87].

```
$ seqkit sort -nN R1_15mer_HD2_UMIs.fasta -o R1_15mer_HD2_UMIs_sorted.fasta
$ seqkit sort -nN R2_15mer_HD2_UMIs.fasta -o R2_15mer_HD2_UMIs_sorted.fasta
```

Step 3) Using pairwise2 (Biopython) local alignment mode with the scoring scheme of (match: 1, mismatch: 0, opening gap: -1, extending gap: -1), IDs that had an alignment score higher than 12 with any other domains' expected 301 bp NGS reads were removed. Also, 10 IDs were chosen to be spread across the 301 bp region as evenly as possible by executing Library1_step3.py.

Step 4) For domains that ended up with fewer than 10 IDs, previously removed IDs with alignment scores (pairwise2) of 13 were recalled and assigned to ensure that the total number of IDs reached 10 for every domain by executing Library1_step4.py. Finally, 10 IDs (R1_15mer_UMIs_10per_effector.fasta and R2_15mer_UMIs_10per_effector.fasta) were generated for each domain.

By matching R1 and R2 reads, a count table for bivalent candidates was generated. We noticed that there was a trend of count numbers for homo-bivalent candidates being higher than hetero-bivalent candidates which might be caused by recombination artifacts. Due to the difficulty in discerning whether the high count number arises from transcriptional perturbation of CD81 or from recombination artifacts, we opted not to analyze homo-bivalent candidates. If the sum of NGS reads from High and Low bins was less than 40 in at least one replicate, the bivalent candidate was considered a dropout. The ratio of a bivalent candidate in a specific bin was calculated by the following formula.

$$Ratio_{bivalent\ candidate\ "i"} = \frac{NGS\ reads_i + 5}{\sum_j^{all\ pairs\ except\ homo-bivalent\ candidates} (NGS\ reads_j + 5)}$$

The enrichment score of bivalent candidate "i" was calculated by dividing $Ratio_{i,CD81\ High\ bin}$ by $Ratio_{i,CD81\ Low\ bin}$.

Secondary validation of individual and bivalent effectors from Library 1

To harness previously ordered effector gene fragments, we again generated a series of landing pad plasmids for nucleofection-based delivery of effectors. For bivalent domain candidates, similar to the library cloning procedure, 3 sequential golden gate reactions were performed. The landing pad plasmid for the 1st golden gate reaction was the same KanR1_receiver (pCM001) as the library cloning, whereas KanR2_individual_validation_receiver (pCM023) was used as the landing pad plasmid for the 2nd golden gate reaction. For the final golden gate reaction, the landing pad was

1048 pCAG_AmpR_backbone (pCM024), which enables the constitutive expression of the effector by
1049 the CAG promoter. For monovalent domain plasmid cloning, 2 sequential golden gate reactions
1050 were performed. For the 1st golden gate reaction, the landing pad plasmid was
1051 KanR_monovalent_receiver (pCM025). For the 2nd golden gate reaction, the landing pad
1052 plasmid was the same as the bivalent domain candidate cloning, pCAG_AmpR_backbone
1053 (pCM024).
1054 For cloning linear gene fragments into KanR1_receiver (pCM001),
1055 KanR2_individual_validation_receiver (pCM023), and KanR_monovalent_receiver (pCM025),
1056 0.25 µL of 60 ng/µL landing pad plasmids, 2.5 µL of 20 nM gene fragment, 0.5 µL of 10X T4
1057 ligase buffer (NEB), 0.25 µL BsaI-HFv2 (NEB, 20000 U/mL), 0.25 µL T4 Ligase (NEB, 400000
1058 U/mL) and 1.25 µL nuclease-free water (Ambion) was mixed well resulting in a total of 5 µL
1059 reaction. The thermocycling condition was 30 cycles of 37°C for 1 min and 16°C for 1 min
1060 followed by 1 cycle of 37°C for 5 min and 75°C for 5 min. For the final golden gate reaction, 0.5
1061 µL of 100 ng/µL pCAG_AmpR_backbone (pCM024), 1 µL of 50 ng/µL N-terminus effector
1062 plasmid, 1 µL of 50 ng/µL C-terminus effector plasmid, 1 µL of FastDigest Esp3I (Thermo Fisher
1063 Scientific), 0.5 µL of T4 DNA ligase (NEB, 400000 U/mL), 1 µL of 10X T4 buffer (NEB), and 5 µL
1064 of nuclease-free water (Ambion) were mixed well resulting in a total of 10 µL reaction.
1065 KanR_monovalent_receiver (pCM025) was used instead of KanR1_receiver (pCM001) or
1066 KanR2_individual_validation_receiver (pCM023) for cloning the monovalent effector plasmid.
1067 The thermocycling protocol was the same: 30 cycles of 37°C for 1 min and 16°C for 1 min
1068 followed by 1 cycle of 37°C for 5 min and 75°C for 5 min.
1069 Nucleofection of effector plasmids was performed with SF Cell Line 4D-Nucleofector X
1070 Kit S following the manufacturer's protocol (4D X-unit, FF-120 program, Lonza). PB Tet-On
1071 dCas9 K562 cell line (with CD81 guide array) was preinduced with 1-2 µg/mL doxycycline
1072 starting 1-3 days before the day of nucleofection. For complete details refer to **Supplementary**
1073 **Table 9**. On the day of measurement, ~300 µL of cells were washed twice with eBioscience
1074 Flow Cytometry Staining Buffer, and 99 µL staining buffer with 1 µL of APC Mouse Anti-Human
1075 CD81 antibody (Cat# 561958, BD Bioscience) was used per well in 96 well plates. Following 1
1076 hour of incubation at 4°C, cells were washed twice, and the CD81 level was measured by
1077 Attune NxT Flow Cytometer (Thermo Fisher Scientific). Empty vector pUC19 nucleofected cells
1078 were used as control cells for gating on BFP, GFP, mCherry, and CD81 (APC) levels.
1079

1080 **Library 2 design, cloning, and barcode mapping**

1081 A literature review was conducted to identify minimally active catalytic epigenetic
1082 effectors across 11 well-established classes: DNA demethylation machinery (DNDM), DNA
1083 methyltransferase (DNMT), E2 and E3 ubiquitin ligases (UBL), histone acetyltransferase (HAT),
1084 histone arginine methyltransferase (HRMT), histone deacetylase (HDAC), histone demethylase
1085 (HDM), histone deubiquitinase (DUB), histone kinase (HK), histone lysine methyltransferase
1086 (HKMT), and histone phosphatase (HP). Human proteins associated with each class were
1087 identified using Gene Ontology terms, except for HKMTs, which were identified as human
1088 proteins containing SET domains in addition to GO terms. Within each list, each protein was
1089 manually reviewed to assess for possible catalytic activity and to search for catalytically active
1090 truncations. In total, 195 catalytic domains were identified across all classes, with approximately
1091 75% sourced directly from literature, while the remaining domain bounds were sourced from

1092 alignment with closely related proteins or simply estimated from Pfam annotations. Additionally,
1093 three non-catalytically active controls were included: RYBP for silencing[36], a 400 aa fragment of
1094 DMD determined to be neutral from HT-recruit[24], and HSF1 for activation[10]. All domains and
1095 references are included in **Supplementary Table 2**.
1096 Amino acid sequences for each effector were codon optimized for human expression
1097 using DNA ChiseI with constraints to avoid restriction enzyme sites (BsaI, BsmBI, BbsI, BtgZI),
1098 avoid patterns (5 x 3-mer, 2 x 15-mer, 2 x 12-mer, 8 x homopolymer), and enforce GC content
1099 between 35-65% in each 50 bp window[81]. Each effector was ordered from Twist Biosciences as
1100 a clonal gene in pTwist Kan High Copy with flanking sequences containing nested BsmBI and
1101 BsaI golden gate sites to facilitate cloning bivalent combinations (**Supplementary Fig. 3a** and
1102 **Supplementary Table 8**, Misc., 5′ and 3′ Effector Flank). All golden gate overhangs were
1103 sourced from a 15 member high fidelity set, and all landing pads contained CcdB dropout genes
1104 to improve cloning efficiency[82]. Individual effector plasmids were transformed into MACH1 cells
1105 (Thermo Fisher Scientific) and miniprepped using QIAprep Spin Miniprep Kit (Qiagen, 27106).
1106 Because lentiviral transduction efficiency decreases roughly 3.5X per additional kilobase of
1107 DNA[29], effector plasmids were pooled exponentially by effector size by manually adding
1108 0.2*3.5^(x/1000) pmol of plasmid DNA, where x is the length of the effector in basepairs
1109 (**Supplementary Fig. 3b**,**c**). The BsmBI sites in this pool (EF2 pool) were later used to clone
1110 into the N-terminal Effector 2 position, and the BsaI sites were used to subclone the pooled
1111 effectors into a new high copy Chloramphenicol resistant backbone via golden gate reaction (50
1112 ng pMH249 (**Supplementary Table 8**, Plasmids), 2-fold molar excess EF2 pool, 1 µL BsaI-
1113 HFv2 (NEB, R3733L), 1 µL T4 ligase (NEB, R0202L), 2.5 µL T4 ligase buffer (NEB, B0202S),
1114 and H_2O to 25 µL incubated at 37°C for 5 min, followed by 30 cycles of 37°C for 5 min and 16°C
1115 for 10 min, followed by final ligation at 16°C for 20 min, final digestion at 37°C for 30 min, and
1116 heat inactivation at 80°C for 20 min) (**Supplementary Fig. 3d**). The reaction was then cleaned
1117 using DNA Clean & Concentrator-5 (Zymo, D4013) and eluted in 6 µL H_2O, before
1118 electroporating 2 µL into 25 µL of Endura electrocompetent cells following the manufacturer's
1119 instructions (Biosearch Technologies, 60242-1). Recovered cells were plated onto a 245 mm x
1120 245 mm plate and incubated overnight at 37°C. The next day, colonies were scraped from the
1121 plate and the plasmid pool was maxiprepped (Machery-Nagel, 740424.50). The resulting EF1
1122 pool contained BsmBI golden gate sites at the same 4 bases as the BsaI insertion of the
1123 effector to allow for subsequent cloning into the C-terminal Effector 1 position (**Supplementary**
1124 **Fig. 3e**).
1125 Before the final bivalent assembly of the EF1 and EF2 pool into our lentiviral landing
1126 pad, the XTEN16 linker and variable barcodes were prepared. The XTEN16 linker was ordered
1127 as two ssDNA oligos with the correct overhangs for assembly between the EF1 and EF2
1128 position and annealed by equimolar mixing at room temperature (**Supplementary Fig. 3f** and
1129 **Supplementary Table 8**, Misc.). Variable barcodes were ordered from Integrated DNA
1130 Technologies (IDT) as a 20xN ssDNA oligo flanked by NGS primer binding sites and BsmBI
1131 golden gate sites for assembly after EF2 (**Supplementary Fig. 3g** and **Supplementary Table**
1132 **8**, Misc.). The oligo was ordered preannealed with the reverse complement of the 3' flanking
1133 sequence to facilitate filling in of the bottom strand of the barcode and 5' flanking sequence by
1134 polymerase extension (2.5 µL of preannealed oligos at 10 uM, 12.5 µL KAPA HiFi HotStart
1135 ReadyMix (Roche KK2601), and H_2O to 25 µL followed by incubation at 98°C for 3 min and

1136 72°C for 30 min). The extended barcode was cleaned with DNA Clean & Concentrator-5 (Zymo,
1137 D4013) and eluted in 20 µL H_2O, before predigestion (1 µg extended barcode, 2 µL Esp3I
1138 (Thermo Fisher Scientific, FD0454), 2 µL 10X FastDigest buffer (Thermo Fisher Scientific, B64),
1139 and H_2O to 20 µL incubated at 37°C for 25 min). The digested barcode was cleaned with DNA
1140 Clean & Concentrator-5 (Zymo, D4013) and diluted to 2 ng/µL. Final bivalent assembly was
1141 performed via 5-piece golden gate reaction into our lentiviral landing pad, which was cloned in
1142 part using the EMMA toolkit[80], containing pTRE3G-MCP-XTEN80 and pSV40-PuroR cassettes
1143 (250 ng pMH276 (**Supplementary Table 8**, Plasmids), 1X molar EF1 pool, 1X molar annealed
1144 XTEN16 linker, 1X molar EF2 pool, 1X molar digested barcode, 1 µL Esp3I (Thermo Scientific,
1145 FD0454), 1 µL T4 ligase (NEB, R0202L), 2.5 µL T4 ligase buffer (NEB, B0202S), and H_2O to 25
1146 µL incubated at 37°C for 5 min, followed by 30 cycles of 37°C for 5 min and 16°C for 10 min,
1147 followed by final ligation at 16°C for 20 min, final digestion at 37°C for 30 min, and heat
1148 inactivation at 80°C for 20 min) (**Supplementary Fig. 3h**). The reaction was then cleaned using
1149 DNA Clean & Concentrator-5 (Zymo, D4013) and eluted in 6 µL H_2O, before electroporating 2x
1150 2 µL into 25 µL of Endura electrocompetent cells each following the manufacturer's instructions
1151 (Biosearch Technologies, 60242-1). Recovered cells were serially diluted and plated onto 100
1152 mm diameter plates for the estimation of colony numbers, while the remaining cells were plated
1153 onto several 245 mm x 245 mm plates. After overnight incubation at 30°C, colonies on dilution
1154 plates were counted, and enough large plates were scraped and maxiprepped (Machery-Nagel,
1155 740424.50) such that the average coverage was between 100-150X colonies per member. Strict
1156 coverage constraints were necessary both to adequately represent shorter effector pairs and to
1157 ensure that there were few enough barcodes to map via long-read sequencing.
1158 Long-read nanopore sequencing was used to map barcodes to bivalent effector pairs.
1159 The plasmid pool was prepared for sequencing using two Cas9 digestion steps followed by
1160 nanopore adapter ligation in an attempt to bias reads towards the barcoded bivalent effector
1161 region (**Supplementary Fig. 3i**). First, two Alt-R *S.p.* Cas9 (IDT, 1081060) RNP pools were
1162 made, one containing the outer guides M1 and P1 and the other containing the inner guides M2
1163 and P2, by prepooling 1 µL of each 100 µM crRNA and following the Alt-R CRISPR-Cas9
1164 System protocol (**Supplementary Table 8**, Guides). The plasmid pool was then digested with
1165 the outer guides M1 and P1 (5 µg plasmid pool, 10 µL M1+P1 Cas9 RNP, 4 µL 10X rCutSmart
1166 buffer (NEB, B6004S), and H_2O to 40 µL incubated at 37°C for 1 hour). The reaction was
1167 stopped by the addition of Proteinase K (+5 µL 20 mg/mL Proteinase K (Zymo, D3001-2-20),
1168 incubated at 56°C for 10 min). A 1X AMPure XP bead (Beckman Coulter, A63881) cleanup was
1169 performed before dephosphorylation of ends followed by second digestion with the inner guides
1170 M2 and P2 (24 µL eluate, 3 µL Quick CIP (NEB, M0525S), and 3 µL 10X rCutSmart buffer
1171 (NEB, B6004S) incubated at 37°C for 10 min and heat inactivated at 80°C for 2 min, followed by
1172 addition of 10 µL M2+P2 Cas9 RNP and incubation at 37°C for 1 hour). The reaction was
1173 stopped by the addition of Proteinase K (+5 µL 20 mg/mL Proteinase K (Zymo, D3001-2-20),
1174 incubated at 56°C for 10 min). A 0.5X AMPure XP bead (Beckman Coulter, A63881) cleanup
1175 was performed before dA tailing using Taq polymerase (34 µL eluate, 1 µL 10 mM dNTP mix
1176 (NEB, N0447S), 1 µL Taq polymerase (NEB, M0267S), and 4 µL 10X rCutSmart buffer (NEB,
1177 B6004S) incubated at 72°C for 5 min). Another 0.5X AMPure XP bead (Beckman Coulter,
1178 A63881) cleanup was performed before nanopore adapter ligation (60 µL eluate, 25 µL Ligation
1179 Buffer (LNB, Oxford Nanopore, SQK-LSK114), 10 µL NEBNext Quick T4 DNA Ligase (NEB,

1180 E6056S), and 5 µL Ligation Adapter (LA, Oxford Nanopore, SQK-LSK114) incubated at room
1181 temperature for 20 min). A final AMPure XP bead (Beckman Coulter, A63881) cleanup was
1182 performed following the SQK-LSK114 protocol using the Short Fragment Buffer (SFB, Oxford
1183 Nanopore, SQK-LSK114). The resulting library was quantified using Qubit 1X dsDNA High
1184 Sensitivity Assay (Invitrogen, Q33231) and diluted to 20 fmol in 12 µL elution buffer (EB, Oxford
1185 Nanopore, SQK-LSK114) for sequencing on a MinION flow cell (Oxford Nanopore, FLO-
1186 MIN114) followed by a PromethION flow cell (Oxford Nanopore, FLO-PRO114M).
1187 Nanopore reads were basecalled and duplexed using Dorado's super-accuracy model
1188 v4.1.0 before conversion to .fastq file format by executing supduplex2fastq.sh on an
1189 appropriately configured GPU virtual machine. Barcode to effector pairings were then mapped
1190 by executing bc_extraction.py. Briefly, Effector 1, Effector 2, and barcode sequences were
1191 extracted from each read using cutadapt and appropriate flanking sequences before effectors
1192 were mapped to individual effectors using minimap2[88,89]. Effector mappings with <75% identity
1193 were discarded. The mapped barcodes from all sequencing runs were then combined into a
1194 single table of unique pairings and filtered to remove any duplicate barcodes
1195 (mappedBCs_filt.csv). In total, 7.8 million barcodes were mapped and represented every
1196 possible bivalent combination with the number of barcodes mapped scaling exponentially by
1197 bivalent effector length (**Supplementary Fig. 3j**,**k**).
1198

1199 **High-throughput assay to measure transcriptional effects of Library 2**

1200 A pooled lentiviral library was generated from Library 2 using the LV-MAX kit (Gibco,
1201 A35348) and protocol in a 1L flask. Lentivirus was concentrated 10X using Lenti-X concentrator
1202 following the manufacturer's instructions (Takara, 631232). Functional titer was measured by
1203 transducing 40,000 K562 cells per well of a 96 well plate with serial dilutions of lentivirus and 8
1204 µg/mL polybrene (Millipore, TR-1003-G) via 90 minute spinfection at 1000g and 32°C. After
1205 overnight incubation, media containing lentivirus was replaced with fresh media and cells were
1206 allowed to recover for another 24 hours before being split equally into media with and without
1207 puromycin (2 µg/mL final, Gibco, A1113803). After five days of selection, cell survival in each
1208 well was quantified on a Tecan Spark plate reader using CellTiter-Glo 2.0 Cell Viability Assay
1209 (Promega, G9242). Percent survival was calculated as the ratio of luminescence in the
1210 presence versus absence of puromycin for each lentiviral dilution, and functional lentiviral titer
1211 was calculated and averaged for all dilutions with 5-30% survival. Two independent full scale
1212 transductions were then performed by transducing the PB Tet-On dCas9 3X CD81 K562 cell
1213 line at 100X library coverage and an MOI <0.1 with 8 µg/mL polybrene (Millipore, TR-1003-G)
1214 via 90 minute spinfection at 1000g and 32°C. After overnight incubation, media containing
1215 lentivirus was replaced with fresh media and cells were allowed to recover for another 24 hours
1216 before starting selection with 2 µg/mL puromycin for 5 days (Gibco, A1113803).
1217 To assess bivalent chromatin effector activity in high-throughput, engineered cells were
1218 induced with 1 µg/mL doxycycline in 200 mL media in a 1L Erlenmeyer flask, maintaining
1219 >1000X library coverage and replacing doxycycline media each day. After 5 days of induction
1220 (Day 0 timepoint), roughly 150 million cells (~3750X coverage) were frozen in 10 mL media
1221 supplemented with 10% DMSO at -80°C in a 15 mL falcon tube. Roughly 50 million remaining
1222 cells (~1250X coverage) were passaged to assess memory by washing twice with DPBS (Gibco
1223 14190144) and resuspending in 400 mL fresh media without doxycycline in a 2L Erlenmeyer

1224 flask. Every 3 days for 24 total days, two frozen stocks of ~3000X cells were made as described
1225 above, and cells were diluted to a minimum density of 1e5/mL in 400 mL media in a 2L
1226 Erlenmeyer flask. Two frozen timepoints, Day 0 and Day 12, were chosen to assess transient
1227 effector activity and epigenetic memory on CD81 (**Supplementary Fig. 6a**). For a given
1228 timepoint and replicate, the frozen aliquot was thawed in a 37°C water bath for 4 min before
1229 being diluted in 35 mL stain buffer (BD, 554656) and pelleted at 300g for 10 min. The cell pellet
1230 was resuspended in 14 mL stain buffer containing 750 µL PE-conjugated CD81 monoclonal
1231 antibody (Invitrogen, MA1-10292), and the tube was rotated for 30 min at 4°C. After staining,
1232 cells were spun down at 300g for 8 min and washed twice with 15 mL stain buffer before
1233 resuspending in 15 mL and straining through a 40 µM filter. Using a BD FACSAria Fusion
1234 Special Order Research Product, between 7-13 million cells were sorted from the top and
1235 bottom 25% of the PE fluorescence distribution (**Supplementary Fig. 8b-d**).
1236 To measure bivalent effector representation in each sorted population, genomic DNA
1237 was harvested using NucleoSpin Blood L kit and protocol (Machery-Nagel, 740954.20), adding
1238 200 µL Monarch RNAse A (NEB, T3018L) before lysis and using high-yield elution
1239 recommendations. Then NGS libraries of bivalent effector barcodes were prepared using two
1240 sequential PCR steps. In PCR1, barcodes were amplified from gDNA using primer pairs
1241 containing staggers to diversity NGS reads (**Supplementary Table 8**, Primers, MH160-MH175)
1242 (up to 100 µg gDNA, 24 µL PCR1 primer set at 50 µM each, 600 µL NEBNext Ultra II Q5 MM
1243 (NEB, M0544L), and H_2O to 1200 µL, divided into 12x 100 µL reactions in a PCR plate and
1244 incubated at 98°C for 30 sec, 20 cycles of 98°C for 10 sec and 65°C for 75 sec, final extension
1245 at 65°C for 5 min). Split reactions were pooled and mixed thoroughly before 25 µL were cleaned
1246 using a two sided AMPure XP bead (Beckman Coulter, A63881) cleanup from 0.7X to 1.8X. In
1247 PCR2, sample indices were added along with flow cell binding sequences p5 and p7 (50-100 ng
1248 purified PCR1, 5 µL PCR2 primer set at 10 µM each, 25 µL NEBNext Ultra II Q5 MM (NEB,
1249 M0544L), and H_2O to 50 µL, incubated at 98°C for 30 sec, 7 cycles of 98°C for 10 sec and 65°C
1250 for 75 sec, final extension at 65°C for 5 min). The reactions were cleaned using a two sided
1251 AMPure XP bead (Beckman Coulter, A63881) cleanup from 0.7X to 1.5X. Each sample was
1252 quantified using Qubit 1X dsDNA High Sensitivity Assay (Invitrogen, Q33231) and 60 ng of each
1253 were pooled into a single NGS library that was sequenced on a NextSeq 2000 using a P3 2x51
1254 cycle paired-end run (Illumina, 20040559).
1255

1256 **Targeted nanopore sequencing to assess barcode swapping in Library 2**

1257 To address the issue of barcode swapping, which is commonly associated with the use
1258 of barcodes in lentiviral libraries[90], Library 2 contained only a short 39 bp homologous sequence
1259 between the end of the effector fusion and the barcode. Still, to quantitatively measure lentiviral
1260 recombination between bivalent effector pairings and barcodes, barcode swapping was
1261 assessed post-integration via long-read nanopore sequencing using Cas9-guided adapter
1262 ligation (**Supplementary Fig. 7a**)[91]. Genomic DNA from one full-scale lentiviral infection
1263 replicate was extracted using Quick-DNA Midiprep Plus kit and protocol (Zymo, D4075). An Alt-
1264 R *S.p.* Cas9 (IDT, 1081060) RNP pool was made by prepooling 1 µL of crRNAs M1, M2, P1,
1265 and P2 at 100 µM and following the Alt-R CRISPR-Cas9 System protocol (**Supplementary**
1266 **Table 8**, Guides). Genomic DNA was dephosphorylated before Cas9 cleavage and dA-tailing (5
1267 µg gDNA, 3 µL Quick CIP (NEB, M0525S), 3 µL 10X rCutSmart buffer (NEB, B6004S), H_2O to

1268 30 µL incubated at 37°C for 10 min and heat inactivated at 80°C for 2 min, followed by addition
1269 of 10 µL M1+M2+P1+P2 Cas9 RNP, 1 µL dATP at 10 mM (NEB, N0440S), and 1 µL Taq
1270 polymerase (NEB, M0267S) and incubation at 37°C for 20 min and 72°C for 5 min). The
1271 reaction was cleaned using AMPure XP beads (Beckman Coulter, A63881) at 0.5X and DNA
1272 eluted in 60 µL H_2O. Nanopore adapters were ligated following the SQK-LSK114 protocol, and
1273 the resulting library was sequenced on a MinION flow cell (Oxford Nanopore, FLO-MIN114).
1274 Nanopore reads were basecalled and converted to .fastq as previously described. Sequences
1275 containing complete reads through both effector positions were extracted using cutadapt and
1276 appropriate flanking sequences[89]. Barcode to effector pairings were mapped using
1277 bc_extraction.py, modified to retain all found barcodes, which were then referenced against
1278 mappedBCs_filt.csv. Reads from any mismatches between barcode to effector pairings were
1279 manually examined to determine the mismatch position (**Supplementary Fig. 7b**).
1280

1281 **NGS analysis of barcodes and bivalent domains from Library 2**

1282 NGS reads were converted into barcode counts using the script count_barcodes.py. In
1283 summary, reads were merged with fastp before barcodes were excised with cutadapt using
1284 forward and reverse NGS primer sequences[88,89]. Then, barcodes were dereplicated and
1285 tabulated using SeqFu, and the results were combined into a single table of barcode
1286 occurrences by experimental condition[92]. After counting, any barcodes that were not mapped to
1287 effector pairs via nanopore were discarded, leaving an average of 76.6% of NGS reads
1288 (**Supplementary Fig. 6e**), and any barcodes containing homopolymer repeats of 8 or more
1289 were discarded due to limitations of nanopore sequencing. Next, barcode counts mapping to the
1290 same effector pair were combined to produce a total read count for each bivalent effector in
1291 each condition. Effector pairs were considered dropouts if there were less than 100 cumulative
1292 reads in both bins in either replicate and/or less than 5 reads in any bin of either replicate to
1293 prevent artifactual inflation or deflation of enrichment scores. Then read counts were normalized
1294 by the sum of each bin, and the enrichment scores were calculated as the ratio of the
1295 normalized counts in the High bin versus the Low bin. The average enrichment score from both
1296 replicates was computed using a geometric mean of the High/Low enrichment ratio.
1297

1298 **Secondary validation of individual and bivalent effectors from Library 2**

1299 Selected individual and bivalent effectors from Library 2 were individually assessed via
1300 transient transfection into the PB Tet-On dCas9 K562 cell line with the 3X CD81 guide array (for
1301 assessing activity on CD81) or without the 3X CD81 guide array (for assessing activity on
1302 additional genes). To clone the constructs for transient transfection, a CcdB dropout landing pad
1303 was first made to assemble the pTRE3G-MCP-XTEN80-effector fusion while also expressing
1304 pEF1a-EGFP-P2A-PuroR in a divergent orientation (**Supplementary Table 8**, Plasmids,
1305 pMH308). The individual clonal effectors ordered from Twist Biosciences were directly used for
1306 insertion into the Effector 2 position via the BsmBI sites in the flanking sequences. To generate
1307 the proper overhangs for insertion into the Effector 1 position, clonal effectors were predigested
1308 with BsaI (600 ng clonal fragment, 1 µL BsaI-HFv2 (NEB, R3733L), 1 µL Quick CIP (NEB,
1309 M0525S), 1 µL 10X rCutSmart buffer (NEB, B6004S), and H_2O to 10 µL incubated at 37°C for 2
1310 hours and 80°C for 1 hour). The same XTEN16 linker was used for bivalent assembly, while an
1311 Effector 2 stuffer was used in place of both Effector 2 and the XTEN16 linker for monovalent

1312 assembly (**Supplementary Table 8**, Misc.). To prepare the XTEN16 linker and Effector 2
1313 stuffer, individual ssDNA oligos were ordered, annealed, and phosphorylated (1 µL 100 µM F
1314 oligo, 1 µL 100 µM R oligo, 1 µL T4 ligase buffer (NEB, B0202S), 1 µL T4 PNK (NEB, M0201S),
1315 and H_2O to 6 µL incubated at 37°C for 30 min, 65°C for 20 min, and 95°C for 5 min before
1316 cooling down to 4°C over 15 min). The final assembly of bivalent effectors was performed using
1317 Golden Gate assembly (50 ng pMH308, 0.5 µL EF1 predigest reaction, 0.2 µL XTEN16 oligo
1318 anneal, 0.5 µL EF2 clonal fragment at ~60 ng/µL, 1 µL T4 ligase buffer (NEB, B0202S), 0.5 µL
1319 Esp3I (Thermo Fisher Scientific, FD0454), 0.5 µL T4 ligase (NEB, R0202L), and H_2O to 10 µL
1320 incubated at 37°C for 5 min, followed by 30 cycles of 37°C for 5 min and 16°C for 10 min,
1321 followed by final ligation at 16°C for 20 min, final digestion at 37°C for 30 min, and heat
1322 inactivation at 80°C for 20 min). The final assembly of monovalent effectors was also performed
1323 using golden gate assembly (50 ng pMH308, 0.5 µL EF1 predigest reaction, 0.2 µL EF2 stuffer
1324 oligo anneal, 1 µL T4 ligase buffer (NEB, B0202S), 0.5 µL Esp3I (Thermo Scientific, FD0454),
1325 0.5 µL T4 ligase (NEB, R0202L), and H_2O to 10 µL incubated at 37°C for 5 min, followed by 30
1326 cycles of 37°C for 5 min and 16°C for 10 min, followed by final ligation at 16°C for 20 min, final
1327 digestion at 37°C for 30 min, and heat inactivation at 80°C for 20 min). 2 µL of each reaction
1328 were transformed into MACH1 cells (Thermo Fisher Scientific) before individual colonies were
1329 picked and grown overnight in 3 mL TB for plasmid purification with NucleoSpin Plasmid
1330 Transfection-grade miniprep kit (Machery-Nagel, 740490). All plasmids were sequence
1331 confirmed via full plasmid nanopore sequencing.
1332 Catalytic mutations for specific effectors were sourced through literature review
1333 (**Supplementary Table 5**). To clone mutations into sequence confirmed individual validation
1334 constructs generated above, 2-3 PCR fragments were made to overlap over the mutation site or
1335 sites and the GFP gene for Gibson assembly of the mutant plasmids (**Supplementary Table 8**,
1336 Primers, MH302-MH345). PCR fragments were generated from corresponding unmutated
1337 plasmids (10 ng parent plasmid, 0.75 µL 10 µM F primer, 0.75 µL 10 µM R primer, 12.5 µL
1338 KAPA HiFi HotStart ReadyMix (Roche, KK2601), H_2O to 10 µL incubated at 95°C for 3 min, 18
1339 cycles of 98°C for 20 sec and 72°C for 3 min, and 72°C for 6 min, followed by addition of 1 µL
1340 DpnI (NEB, R0176S) and incubation at 37°C for 1 hour and 80°C for 20 min). 2 µL of the
1341 resulting reactions were analyzed for product length and purity via gel electrophoresis before
1342 mutant plasmids were assembled via Gibson assembly (1 µL each corresponding PCR reaction,
1343 10 µL 2X Gibson MM, and H_2O to 10 µL incubated at 50°C for 1 hour). 2 µL of each reaction
1344 were transformed into MACH1 cells (Thermo Fisher Scientific) before individual colonies were
1345 picked and grown overnight in 3 mL TB for plasmid purification with NucleoSpin Plasmid
1346 Transfection-grade miniprep kit (Machery-Nagel, 740490). All mutant plasmids were sequence
1347 confirmed via full plasmid nanopore sequencing.
1348 Sequence confirmed validation plasmids were nucleofected into the PB Tet-On dCas9
1349 K562 cell lines using SF Cell Line 96-well Nucleofector kit (Lonza, V4SC-2096). The
1350 manufacturer's instructions were followed using 800 ng plasmid DNA per nucleofection. For
1351 testing effectors on CD81, only the effector plasmid was nucleofected into the Tet-On dCas9
1352 cell line with the 3X CD81 guide array. For testing effectors on additional genes, the effector
1353 plasmid and the corresponding 3X guide array plasmid were nucleofected at a 1:1 mass ratio
1354 into the Tet-On dCas9 cell line without the 3X CD81 guide array. After nucleofection, cells were
1355 plated directly into 1 µg/mL final concentration of doxycycline to induce dCas9 and MCP-effector

expression. One day after nucleofection and every subsequent day until 5 days post-nucleofection, media was replaced with fresh media containing 1 µg/mL doxycycline and 2 µg/mL puromycin (Gibco, A1113803). Five days post-nucleofection, cells were analyzed for transient effector activity on the gene target by transferring to 96 well U-bottom plates and spinning down at 300g for 3 min. Media was aspirated, and cells were resuspended in 100 µL stain buffer (BD, 554656) per well. Then 100 µL stain buffer containing 1.25 µL fluorescently conjugated antibody was added to each well and mixed by pipetting before incubation at 4°C for 30 min (APC CD55 antibody (Biolegends, 311311), Alexa Fluor 647 CD58 antibody (BD Pharmingen, 563567), PE CD81 antibody (Invitrogen, MA1-10292), APC CD151 antibody (Biolegends, 350405), and APC CD155 antibody (eBioscience, 2H7CD155). After incubation, cells were washed twice with 200 µL stain buffer before final resuspension in 200 µL stain buffer per well. Stained cells were analyzed by flow cytometry on an Attune NxT Flow Cytometer (Thermo Fisher Scientific). To assess for long-term effector activity, cells at five days post-nucleofection were transferred to 96 well V-bottom plates and washed twice with 200 µL DPBS (Gibco, 14190144) per well before resuspending in fresh media without doxycycline or puromycin. Three days later and at subsequent timepoints, cells were split to maintain growth, and the remaining cells were stained and analyzed as above.

To systematically analyze large batches of flow cytometry data, Cytoflow's Jupyter notebook integration was used[93]. Live and singlet gates were first defined on WT K562 cells measured using the same cytometer settings, and the gates were applied to each sample file. Then, for transient timepoint analysis, cells were further gated for BFP and GFP, indicating dCas9 expression and the presence of the MCP-effector plasmid. Transient timepoints on genes other than CD81 were also gated on mCherry, indicating the presence of the 3X guide array plasmid. Threshold gates were defined at the 99.9th percentile of the channel measurements in WT K562 cells. For memory timepoints, no gating beyond live and singlet gates was performed. After gating, mean fluorescence intensity (MFI) was calculated for each sample using the flow.geom_mean function in Cytoflow on the channel corresponding to the fluorescent antibody. Percent change in MFI was calculated using the MFI from the neutral DMD control as a reference. Percent cells activated and percent cells repressed were calculated using threshold gating at the 1st and 99th percentile of the neutral DMD control effector, and the percent cells silenced was calculated using threshold gating at the 99th percentile of unstained WT K562 cells.

Analysis of individual and bivalent effector strength

To calculate the total number of significant effector pairs for each library, the raw count matrices were analyzed with pyDESeq2[94] which corresponds to DESeq2 (v1.34.0) with single-factor analysis, Wald tests, and LFC shrinkage mode (**Supplementary Tables 3** and **4**). For screen 1, candidates with total NGS reads of at least 80 were analyzed. For screen 2, the total NGS reads threshold was set as 100. Threshold for statistical significance was set as $|\log2FC| > 1$ and $p_{adjusted} < 0.05$.

A marginal effect test was defined to assess the marginal, or average, effect of a given individual effector. To conduct the test for a given effector, the bivalent pairs and corresponding average fold enrichment scores were split into two groups, those containing the effector and those not containing the effector. The marginal score was defined as the difference in mean fold enrichment between the two groups, and if ≥ 30 pairs were present in both groups, a Welsh's t-test was conducted. It was determined that a difference of means t-test was necessary, rather

than a one sample t-test, to correct for library composition bias. In other words, the mean fold enrichment of any given individual effector would naturally be positive or negative if the overall library had a bias in either direction simply because the given effector is paired with every other library member. A Welsh's t-test was chosen as opposed to a Student's t-test because it was expected that individual effectors may vary in their interactions with other library members, thus not only altering the mean fold enrichment but also the standard deviation of fold enrichment scores. Once all the effectors were analyzed, p-values were corrected for a false discovery rate of 5%.

Synergy scoring to identify synergistic and antagonistic combinations

To identify bivalent combinations with unexpected activities, synergy scores were calculated for each bivalent combination based on the expected effects of each individual effector (**Fig. 4a**). First, the individual effects of each effector were calculated using our marginal score metric, with the difference that each effector was scored for both the N-terminal and C-terminal position. Then, the sum of the corresponding marginal scores for each bivalent combination was computed. Because effectors could still be additive in nature even if the measured score did not exactly match the sum, a range for additive activity was defined that assumes that effectors may not contribute their full marginal strength to the combination but that the contribution of each effector should still be in the expected direction. For expected repressors, the lower bound of the additive range was defined as the minimum of the N-terminal marginal score, the C-terminal marginal score, and the sum of the marginal scores (min(N-term, C-term, Sum)), and the upper bound of the range was defined as the maximum of the sum of the marginal scores and the minimum of the two marginal scores (max(Sum, min(N-term, C-term))). For expected activators, the expressions are reversed and the additive range becomes (min(Sum, max(N-term, C-term))) to (max(N-term, C-term, Sum)). Log_2 fold enrichment scores from HTS data were first mean centered, a logical step considering that marginal scores are relative contributions and are unaffected by central tendency, and subsequently compared to the additive range. In all cases, if the observed data fell within the additive range, the pair was considered additive and assigned a synergy score of 0. For expected repressors, bivalent combinations were considered "synergistic" if the measured score fell below the additive range, i.e. it was more repressive than expected, and the combination was considered "antagonistic" if the measured score fell above the additive range, i.e. it was less repressive than expected. Scores for expected activators were determined in the same way but in the opposite direction, with synergistic combinations exhibiting unexpectedly high observed scores and antagonistic combinations exhibiting unexpectedly low observed scores. In both cases, the synergy score was defined as how far outside the additive range the observed score fell, being positive for synergy and negative for antagonism. Because Library 1 was entirely composed of expected repressors, every combination was scored as a repressor. For Library 2, the sum of the marginal scores determined whether the combination was scored as an activator or a repressor with positive sums being scored as expected activators and negative sums being scored as expected repressors.

To test if individual effectors broadly synergize or antagonize with KRAB members from Library 1 or HDAC members from Library 2, the synergy scores from all combinations containing the given effector with a KRAB or HDAC member were tested against the null hypothesis that the average synergy score was zero using a one-sample Wilcoxon test. Only

1447 KRAB or HDAC members with marginal scores less than -0.5 were considered, and p-values
1448 were subsequently FDR corrected for multiple hypothesis testing. In addition to performing
1449 significance testing, the average synergy score and the average $\log_2$ fold enrichment score for
1450 the combinations were calculated.
1451

1452 **Comparison between stdMCP-KRAB and stdMCP-KRAB-L3MBTL3**

1453 pTRE3G-PuroR-T2A-stdMCP-XTEN80-KRAB(ZNF10)-L3MBTL3-WPRE and pTRE3G-PuroR-
1454 T2A-stdMCP-XTEN80-KRAB(ZNF10)-WPRE were infected by lentivirus to Tet-On dCas9 K562
1455 (without CD81 guide array) in similar MOI (0.35 ± 0.04 for KRAB-L3MBTL3 and 0.31 ± 0.01 for
1456 KRAB). For comparing across different panels of genes and guides, an equal amount of
1457 lentivirus encoding both sgRNA and mCherry marker were infected to both cell lines.
1458 Doxycycline concentration was maintained at 1-2 μg/mL since the LV-sgRNA infection. 5 days
1459 after lentiviral infection of sgRNAs, cells were stained with corresponding antibodies (APC anti-
1460 human CD55 antibody (Cat# 311311, Biolegends), Alexa Fluor 647 Mouse Anti-Human CD58
1461 antibody (Cat# 563567, BD Pharmingen), APC Mouse Anti-Human CD81 antibody (Cat#
1462 561958, BD Bioscience), and APC anti-human CD151 antibody (Cat# 350405, Biolegends)) and
1463 expression level was measured by Attune NxT Flow Cytometer (Thermo Fisher Scientific). For
1464 the bidirectional perturbations using the MS2/PP7 system, pTREtight-stdPCP-p65-HSF1-T2A-
1465 BFP were lentivirally infected to the previous two cell lines described above. pTREtight-stdPCP-
1466 p65-HSF1-T2A-BFP was cloned from the construct pHR-CMV-stdPCP-p65-HSF1-T2A-GFP
1467 (Addgene #199456)[62]. The same amounts of lentivirus encoding both mouse U6 promoter-
1468 driven 2x MS2 sgRNA and human U6 promoter-driven 2x PP7 sgRNA were infected to both cell
1469 lines. Doxycycline concentration was maintained at 1-2 μg/mL since the day of LV-dual
1470 MS2/PP7 sgRNAs infection. CD81/CD274 expression profiles were measured 5 days post-
1471 infection of dual MS2/PP7 sgRNAs following staining with antibodies against both targets (APC
1472 Mouse Anti-Human CD81 antibody (Cat# 561958, BD Bioscience) and Alexa Fluor 488 Mouse
1473 Anti-Human CD274 antibody (Cat# 53-5983-42, Invitrogen)) by Attune NxT Flow Cytometer
1474 (Thermo Fisher Scientific).

Table of Contents for Supplementary Information

1. **Supplementary Figures**
    1. Classifications and size distributions of individual domains from Library 1 and Library 2
    2. Library 1 combinatorial cloning strategy
    3. Library 2 combinatorial cloning and barcode mapping strategy
    4. Doxycycline-inducible dCas9/MS2 system enables temporal control of transcriptional perturbation
    5. Detailed procedures for Library 1 HTS
    6. Detailed procedures for Library 2 HTS and barcode mapping
    7. Investigation of lentiviral barcode swapping by targeted nanopore sequencing
    8. Number of acquired NGS reads versus bivalent effector length
    9. Heatmaps of enrichment scores from later HTS timepoints
    10. N- versus C-terminal position effects
    11. Synergy score heatmaps highlight synergistic and antagonistic interactions in Library 1
    12. Synergy score heatmaps highlight synergistic and antagonistic interactions in Library 2
    13. Synergistic interaction between the H2AK119ub1 reader and a subset of PRC1 recruiters
    14. HDAC and KRAB members included in the average synergy score calculation
    15. Epigenetic modifications at CD81 locus
    16. Key effectors from Library 2 transiently perturb CD55, CD58, CD151, and CD155
    17. Gene-by-gene scatter plots of percent change in MFI induced by key effectors from Library 2
    18. Synergistic partners of KRAB and antagonistic partners of KRAB and SID4X
    19. Quantification of bidirectional perturbations by MS2/PP7 system
    20. Marginal effector and synergy score analysis on Day 12
    21. DNMT3A-3L combinations induce long-term partial silencing of CD81
    22. UBE2E1 + DNMT3A induces long-term repression of CD81
    23. Violin plot timecourses of TET1 combinations
    24. TET1 combinations induce long-term activation of CD81
2. **Supplementary Note**
    1. Synergistic interaction between the H2AK119ub1 reader and a subset of PRC1 recruiters
3. **Supplementary Tables**

1. Library 1 members and sequences
2. Library 2 members and sequences
3. Library 1 HTS results
4. Library 2 HTS results
5. Catalytic mutations
6. Library 1 synergy scores
7. Library 2 synergy scores
8. Plasmid, primer, and guide sequences
9. Library 1 individual validation details

Data availability

All data to support the results are in the main text, figures and supplementary tables. Illumina and Nanopore sequencing datasets generated in this study will be available on the NCBI Sequence Read Archive, Bioproject PRJNA1143488.

Code availability

The code for analyses performed in this paper will be available on GitHub.

Acknowledgments

We thank the entire Hsu lab for helpful discussions and feedback, as well as B. Plosky and the Arc Institute Scientific Publications Team for assistance with the manuscript. P.D.H. is supported by funding from the Arc Institute, Yosemite, the Biswas Foundation, the Rainwater Foundation, the Curci Foundation, the Rose Hill Innovators Program, S. Altman, V. and N. Khosla, and by anonymous gifts to the Hsu Laboratory.

Competing Interests

P.D.H. is a cofounder of Stylus Medicine, Circle Labs, and Spotlight Therapeutics, serves on the board of directors at Stylus Medicine, is a board observer at EvolutionaryScale, Circle Labs, and Spotlight Therapeutics, a scientific advisory board member at Arbor Biosciences and Veda Bio, and an advisor to NFDG, Varda Space, and Vial Health.

Author Contributions

H.C.M., M.H.H., and P.D.H. conceived the study. H.C.M., M.H.H., S.K., and P.D.H. designed experiments. H.C.M. and M.H.H. performed experiments and computational analyses. P.D.H. and S.K. supervised the research. H.C.M., M.H.H., A.P., S.K., and P.D.H. wrote the manuscript.

1548 # References

1549 1. Goldberg, A. D., Allis, C. D. & Bernstein, E. Epigenetics: a landscape takes shape. *Cell*
1550 **128**, 635–638 (2007).
1551 2. Vogelauer, M., Rubbi, L., Lucas, I., Brewer, B. J. & Grunstein, M. Histone acetylation
1552 regulates the time of replication origin firing. *Mol. Cell* **10**, 1223–1233 (2002).
1553 3. Hauer, M. H. & Gasser, S. M. Chromatin and nucleosome dynamics in DNA damage and
1554 repair. *Genes Dev.* **31**, 2204–2221 (2017).
1555 4. Zhang, T., Cooper, S. & Brockdorff, N. The interplay of histone modifications – writers that
1556 read. *EMBO Rep.* **16**, 1467-1481–1481 (2015).
1557 5. Policarpi, C., Munafò, M., Tsagkris, S., Carlini, V. & Hackett, J. A. Systematic epigenome
1558 editing captures the context-dependent instructive function of chromatin modifications. *Nat.*
1559 *Genet.* **56**, 1168–1180 (2024).
1560 6. Lukauskas, S. *et al.* Decoding chromatin states by proteomic profiling of nucleosome
1561 readers. *Nature* **627**, 671–679 (2024).
1562 7. Kuzmichev, A., Nishioka, K., Erdjument-Bromage, H., Tempst, P. & Reinberg, D. Histone
1563 methyltransferase activity associated with a human multiprotein complex containing the
1564 Enhancer of Zeste protein. *Genes Dev.* **16**, 2893–2905 (2002).
1565 8. Thakore, P. I., Black, J. B., Hilton, I. B. & Gersbach, C. A. Editing the epigenome:
1566 technologies for programmable transcription and epigenetic modulation. *Nat. Methods* **13**,
1567 127–137 (2016).
1568 9. Nakamura, M., Gao, Y., Dominguez, A. A. & Qi, L. S. CRISPR technologies for precise
1569 epigenome editing. *Nat. Cell Biol.* **23**, 11–22 (2021).
1570 10. Konermann, S. *et al.* Genome-scale transcriptional activation by an engineered CRISPR-
1571 Cas9 complex. *Nature* **517**, 583–588 (2015).
1572 11. Amabile, A. *et al.* Inheritable Silencing of Endogenous Genes by Hit-and-Run Targeted
1573 Epigenetic Editing. *Cell* **167**, 219-232.e14 (2016).

1574 12. Nuñez, J. K. *et al.* Genome-wide programmable transcriptional memory by CRISPR-based
1575 epigenome editing. *Cell* **184**, 2503-2519.e17 (2021).
1576 13. Cappelluti, M. A. *et al.* Durable and efficient gene silencing in vivo by hit-and-run
1577 epigenome editing. *Nature* **627**, 416–423 (2024).
1578 14. Konermann, S. *et al.* Optical control of mammalian endogenous transcription and
1579 epigenetic states. *Nature* **500**, 472–476 (2013).
1580 15. Chavez, A. *et al.* Highly efficient Cas9-mediated transcriptional programming. *Nat. Methods*
1581 **12**, 326–328 (2015).
1582 16. Bintu, L. *et al.* Dynamics of epigenetic regulation at the single-cell level. *Science* **351**, 720–
1583 724 (2016).
1584 17. Stepper, P. *et al.* Efficient targeted DNA methylation with chimeric dCas9-Dnmt3a-Dnmt3L
1585 methyltransferase. *Nucleic Acids Res.* **45**, 1703–1713 (2017).
1586 18. Yeo, N. C. *et al.* An enhanced CRISPR repressor for targeted mammalian gene regulation.
1587 *Nat. Methods* **15**, 611–616 (2018).
1588 19. O'Geen, H. *et al.* Ezh2-dCas9 and KRAB-dCas9 enable engineering of epigenetic memory
1589 in a context-dependent manner. *Epigenetics Chromatin* **12**, 26 (2019).
1590 20. Alerasool, N., Segal, D., Lee, H. & Taipale, M. An efficient KRAB domain for CRISPRi
1591 applications in human cells. *Nat. Methods* **17**, 1093–1096 (2020).
1592 21. Van, M. V., Fujimori, T. & Bintu, L. Nanobody-mediated control of gene expression and
1593 epigenetic memory. *Nat. Commun.* **12**, 537 (2021).
1594 22. Qian, J. *et al.* Multiplex epigenome editing of MECP2 to rescue Rett syndrome neurons.
1595 *Sci. Transl. Med.* **15**, eadd4666 (2023).
1596 23. Neumann, E. N. *et al.* Brainwide silencing of prion protein by AAV-mediated delivery of an
1597 engineered compact epigenetic editor. *Science* **384**, ado7082 (2024).
1598 24. Tycko, J. *et al.* High-Throughput Discovery and Characterization of Human Transcriptional
1599 Effectors. *Cell* **183**, 2020-2035.e16 (2020).

1600 25. Alerasool, N., Leng, H., Lin, Z.-Y., Gingras, A.-C. & Taipale, M. Identification and functional
1601 characterization of transcriptional activators in human cells. *Mol. Cell* **82**, 677-695.e7
1602 (2022).
1603 26. DelRosso, N. *et al.* Large-scale mapping and mutagenesis of human transcriptional effector
1604 domains. *Nature* **616**, 365–372 (2023).
1605 27. Mukund, A. X. *et al.* High-throughput functional characterization of combinations of
1606 transcriptional activators and repressors. *Cell Syst* **14**, 746-763.e5 (2023).
1607 28. Blaeschke, F. *et al.* Modular pooled discovery of synthetic knockin sequences to program
1608 durable cell therapies. *Cell* **186**, 4216-4234.e33 (2023).
1609 29. Sweeney, N. P. & Vink, C. A. The impact of lentiviral vector genome size and producer cell
1610 genomic to gag-pol mRNA ratios on packaging efficiency and titre. *Mol Ther Methods Clin*
1611 *Dev* **21**, 574–584 (2021).
1612 30. Gohl, D. M. *et al.* Measuring sequencer size bias using REcount: a novel method for highly
1613 accurate Illumina sequencing-based quantification. *Genome Biol.* **20**, 85 (2019).
1614 31. Peabody, D. S. The RNA binding site of bacteriophage MS2 coat protein. *EMBO J.* **12**,
1615 595–600 (1993).
1616 32. Heidersbach, A. J., Dorighi, K. M., Gomez, J. A., Jacobi, A. M. & Haley, B. A versatile, high-
1617 efficiency platform for CRISPR-based gene activation. *Nat. Commun.* **14**, 902 (2023).
1618 33. Wu, B. *et al.* Synonymous modification results in high-fidelity gene expression of repetitive
1619 protein and nucleotide sequences. *Genes Dev.* **29**, 876–886 (2015).
1620 34. Head, S. R. *et al.* Library construction for next-generation sequencing: overviews and
1621 challenges. *Biotechniques* **56**, 61–4, 66, 68, passim (2014).
1622 35. Gordon, K. S. *et al.* Screening for CD19-specific chimaeric antigen receptors with enhanced
1623 signalling via a barcoded library of intracellular domains. *Nat Biomed Eng* **6**, 855–866
1624 (2022).
1625 36. Zhao, J. *et al.* RYBP/YAF2-PRC1 complexes and histone H1-dependent chromatin

1626 compaction mediate propagation of H2AK119ub1 during cell division. *Nat. Cell Biol.* **22**,
1627 439–452 (2020).
1628 37. Ogryzko, V. V., Schiltz, R. L., Russanova, V., Howard, B. H. & Nakatani, Y. The
1629 transcriptional coactivators p300 and CBP are histone acetyltransferases. *Cell* **87**, 953–959
1630 (1996).
1631 38. Lahn, B. T. *et al.* Previously uncharacterized histone acetyltransferases implicated in
1632 mammalian spermatogenesis. *Proc. Natl. Acad. Sci. U. S. A.* **99**, 8707–8712 (2002).
1633 39. Champagne, N., Pelletier, N. & Yang, X. J. The monocytic leukemia zinc finger protein
1634 MOZ is a histone acetyltransferase. *Oncogene* **20**, 404–409 (2001).
1635 40. Guelman, S. *et al.* The double-histone-acetyltransferase complex ATAC is essential for
1636 mammalian development. *Mol. Cell. Biol.* **29**, 1176–1188 (2009).
1637 41. Wei, W. *et al.* Class I histone deacetylases are major histone decrotonylases: evidence for
1638 critical and broad function of histone crotonylation in transcription. *Cell Res.* **27**, 898–915
1639 (2017).
1640 42. Gilbert, L. A. *et al.* CRISPR-mediated modular RNA-guided regulation of transcription in
1641 eukaryotes. *Cell* **154**, 442–451 (2013).
1642 43. Cong, L., Zhou, R., Kuo, Y.-C., Cunniff, M. & Zhang, F. Comprehensive interrogation of
1643 natural TALE DNA-binding modules and transcriptional repressor domains. *Nat. Commun.*
1644 **3**, 968 (2012).
1645 44. Knight, M. J., Leettola, C., Gingery, M., Li, H. & Bowie, J. U. A human sterile alpha motif
1646 domain polymerizome. *Protein Sci.* **20**, 1697–1706 (2011).
1647 45. Xu, T. *et al.* RBPJ/CBF1 interacts with L3MBTL3/MBT1 to promote repression of Notch
1648 signaling via histone demethylase KDM1A/LSD1. *EMBO J.* **36**, 3232–3249 (2017).
1649 46. Schuetz, A. *et al.* Human HDAC7 harbors a class IIa histone deacetylase-specific zinc
1650 binding motif and cryptic deacetylase activity. *J. Biol. Chem.* **283**, 11355–11363 (2008).
1651 47. Wang, A. H. *et al.* HDAC4, a human histone deacetylase related to yeast HDA1, is a

1652 transcriptional corepressor. *Mol. Cell. Biol.* **19**, 7816–7827 (1999).
1653 48. Grazini, U. *et al.* The RING domain of RAG1 ubiquitylates histone H3: a novel activity in
1654 chromatin-mediated regulation of V(D)J joining. *Mol. Cell* **37**, 282–293 (2010).
1655 49. Deng, Z., Liu, H. & Liu, X. RAG1-mediated ubiquitylation of histone H3 is required for
1656 chromosomal V(D)J recombination. *Cell Res.* **25**, 181–192 (2015).
1657 50. Wheaton, K. *et al.* UbE2E1/UBCH6 Is a Critical in Vivo E2 for the PRC1-catalyzed
1658 Ubiquitination of H2A at Lys-119. *J. Biol. Chem.* **292**, 2893–2902 (2017).
1659 51. Weirich, S., Kudithipudi, S. & Jeltsch, A. Specificity of the SUV4–20H1 and SUV4–20H2
1660 protein lysine methyltransferases and methylation of novel substrates. *J. Mol. Biol.* **428**,
1661 2344–2358 (2016).
1662 52. Yurchenko, V., Xue, Z. & Sadofsky, M. The RAG1 N-terminal domain is an E3 ubiquitin
1663 ligase. *Genes Dev.* **17**, 581–585 (2003).
1664 53. Sun, L. & Fang, J. E3-Independent Constitutive Monoubiquitination Complements Histone
1665 Methyltransferase Activity of SETDB1. *Mol. Cell* **62**, 958–966 (2016).
1666 54. Wu, H. *et al.* Crystal structures of the human histone H4K20 methyltransferases SUV420H1
1667 and SUV420H2. *FEBS Lett.* **587**, 3859–3868 (2013).
1668 55. Kang, T.-H. *et al.* Mitotic histone H3 phosphorylation by vaccinia-related kinase 1 in
1669 mammalian cells. *Mol. Cell. Biol.* **27**, 8533–8546 (2007).
1670 56. Kent, W. J. *et al.* The human genome browser at UCSC. *Genome Res.* **12**, 996–1006
1671 (2002).
1672 57. Conway, E. *et al.* A Family of Vertebrate-Specific Polycombs Encoded by the
1673 LCOR/LCORL Genes Balance PRC2 Subtype Activities. *Mol. Cell* **70**, 408-421.e8 (2018).
1674 58. Zhang, Q. *et al.* PALI1 facilitates DNA and nucleosome binding by PRC2 and triggers an
1675 allosteric activation of catalysis. *Nat. Commun.* **12**, 4592 (2021).
1676 59. Fong, K.-W. *et al.* PALI1 promotes tumor growth through competitive recruitment of PRC2
1677 to G9A-target chromatin for dual epigenetic silencing. *Mol. Cell* **82**, 4611-4626.e7 (2022).

1678 60. Zalatan, J. G. *et al.* Engineering complex synthetic transcriptional programs with CRISPR
1679 RNA scaffolds. *Cell* **160**, 339–350 (2015).
1680 61. Martella, A. *et al.* Systematic Evaluation of CRISPRa and CRISPRi Modalities Enables
1681 Development of a Multiplexed, Orthogonal Gene Activation and Repression System. *ACS*
1682 *Synth. Biol.* **8**, 1998–2006 (2019).
1683 62. Liang, Y. *et al.* Gene activation guided by nascent RNA-bound transcription factors. *Nat.*
1684 *Commun.* **13**, 7329 (2022).
1685 63. Boettcher, M. *et al.* Dual gene activation and knockout screen reveals directional
1686 dependencies in genetic networks. *Nat. Biotechnol.* **36**, 170–178 (2018).
1687 64. Pacalin, N. M. *et al.* Bidirectional epigenetic editing reveals hierarchies in gene regulation.
1688 *Nat. Biotechnol.* (2024) doi:10.1038/s41587-024-02213-3.
1689 65. Gowher, H. & Jeltsch, A. Enzymatic properties of recombinant Dnmt3a DNA
1690 methyltransferase from mouse: the enzyme modifies DNA in a non-processive manner and
1691 also methylates non-CpA sites1 1Edited by J. Karn. *J. Mol. Biol.* **309**, 1201–1208 (2001).
1692 66. Jurkowska, R. Z. *et al.* Formation of nucleoprotein filaments by mammalian DNA
1693 methyltransferase Dnmt3a in complex with regulator Dnmt3L. *Nucleic Acids Res.* **36**, 6656–
1694 6663 (2008).
1695 67. Liu, X. S. *et al.* Editing DNA Methylation in the Mammalian Genome. *Cell* **167**, 233-247.e17
1696 (2016).
1697 68. Tahiliani, M. *et al.* Conversion of 5-methylcytosine to 5-hydroxymethylcytosine in
1698 mammalian DNA by MLL partner TET1. *Science* **324**, 930–935 (2009).
1699 69. Liu, X. S. *et al.* Rescue of Fragile X Syndrome Neurons by DNA Methylation Editing of the
1700 FMR1 Gene. *Cell* **172**, 979-992.e6 (2018).
1701 70. Xu, X. *et al.* A CRISPR-based approach for targeted DNA demethylation. *Cell Discov* **2**,
1702 16009 (2016).
1703 71. Choudhury, S. R., Cui, Y., Lubecka, K., Stefanska, B. & Irudayaraj, J. CRISPR-dCas9

1704 mediated TET1 targeting for selective DNA demethylation at BRCA1 promoter. *Oncotarget*
1705 **7**, 46545–46556 (2016).
1706 72. Jenkins, Y. *et al.* Critical role of the ubiquitin ligase activity of UHRF1, a nuclear RING
1707 finger protein, in tumor cell growth. *Mol. Biol. Cell* **16**, 5621–5629 (2005).
1708 73. Blazer, L. L. *et al.* PR Domain-containing Protein 7 (PRDM7) Is a Histone 3 Lysine 4
1709 Trimethyltransferase. *J. Biol. Chem.* **291**, 13509–13519 (2016).
1710 74. Liu, X. *et al.* UHRF1 targets DNMT1 for DNA methylation through cooperative binding of
1711 hemi-methylated DNA and methylated H3K9. *Nat. Commun.* **4**, 1563 (2013).
1712 75. Nishiyama, A. *et al.* Uhrf1-dependent H3K23 ubiquitylation couples maintenance DNA
1713 methylation and replication. *Nature* **502**, 249–253 (2013).
1714 76. Qin, W. *et al.* DNA methylation requires a DNMT1 ubiquitin interacting motif (UIM) and
1715 histone ubiquitination. *Cell Res.* **25**, 911–929 (2015).
1716 77. Li, T. *et al.* Structural and mechanistic insights into UHRF1-mediated DNMT1 activation in
1717 the maintenance DNA methylation. *Nucleic Acids Res.* **46**, 3218–3231 (2018).
1718 78. Dukatz, M. *et al.* Mechanistic Insights into Cytosine-N3 Methylation by DNA
1719 Methyltransferase DNMT3A. *J. Mol. Biol.* **431**, 3139–3145 (2019).
1720 79. Labun, K. *et al.* CHOPCHOP v3: expanding the CRISPR web toolbox beyond genome
1721 editing. *Nucleic Acids Res.* **47**, W171–W174 (2019).
1722 80. Martella, A., Matjusaitis, M., Auxillos, J., Pollard, S. M. & Cai, Y. EMMA: An Extensible
1723 Mammalian Modular Assembly Toolkit for the Rapid Design and Production of Diverse
1724 Expression Vectors. *ACS Synth. Biol.* **6**, 1380–1392 (2017).
1725 81. Zulkower, V. & Rosser, S. DNA Chisel, a versatile sequence optimizer. *Bioinformatics* **36**,
1726 4508–4509 (2020).
1727 82. Potapov, V. *et al.* Comprehensive Profiling of Four Base Overhang Ligation Fidelity by T4
1728 DNA Ligase and Application to DNA Assembly. *ACS Synth. Biol.* **7**, 2665–2674 (2018).
1729 83. Joung, J. *et al.* Genome-scale CRISPR-Cas9 knockout and transcriptional activation

1730 screening. *Nat. Protoc.* **12**, 828–863 (2017).
1731 84. Naik, T., Sharda, M., C P, L., Virbhadra, K. & Pandit, A. High-quality single amplicon
1732 sequencing method for illumina MiSeq platform using pool of 'N' (0–10) spacer-linked target
1733 specific primers without PhiX spike-in. *BMC Genomics* **24**, 141 (2023).
1734 85. Tan, G., Opitz, L., Schlapbach, R. & Rehrauer, H. Long fragments achieve lower base
1735 quality in Illumina paired-end sequencing. *Sci. Rep.* **9**, 2856 (2019).
1736 86. Chen, S., He, C., Li, Y., Li, Z. & Melançon, C. E. A computational toolset for rapid
1737 identification of SARS-CoV-2, other viruses and microorganisms from sequencing data.
1738 *Brief. Bioinform.* **22**, 924–935 (2021).
1739 87. Shen, W., Sipos, B. & Zhao, L. SeqKit2: A Swiss army knife for sequence and alignment
1740 processing. *Imeta* (2024) doi:10.1002/imt2.191.
1741 88. Chen, S., Zhou, Y., Chen, Y. & Gu, J. fastp: an ultra-fast all-in-one FASTQ preprocessor.
1742 *Bioinformatics* **34**, i884–i890 (2018).
1743 89. Martin, M. Cutadapt removes adapter sequences from high-throughput sequencing reads.
1744 *EMBnet.journal* **17**, 10–12 (2011).
1745 90. Sack, L. M., Davoli, T., Xu, Q., Li, M. Z. & Elledge, S. J. Sources of Error in Mammalian
1746 Genetic Screens. *G3* **6**, 2781–2790 (2016).
1747 91. Gilpatrick, T. *et al.* Targeted nanopore sequencing with Cas9-guided adapter ligation. *Nat.*
1748 *Biotechnol.* **38**, 433–438 (2020).
1749 92. Telatin, A., Fariselli, P. & Birolo, G. SeqFu: A Suite of Utilities for the Robust and
1750 Reproducible Manipulation of Sequence Files. *Bioengineering (Basel)* **8**, (2021).
1751 93. Teague, B. Cytoflow: A Python Toolbox for Flow Cytometry. *bioRxiv* 2022.07.22.501078
1752 (2022) doi:10.1101/2022.07.22.501078.
1753 94. Muzellec, B., Teleńczuk, M., Cabeli, V. & Andreux, M. PyDESeq2: a python package for
1754 bulk RNA-seq differential expression analysis. *Bioinformatics* **39**, (2023).
1755 95. Grewal, S. I. S. The molecular basis of heterochromatin assembly and epigenetic

1756 inheritance. *Mol. Cell* **83**, 1767–1785 (2023).